

Stress analyses of a smart composite pipe joint integrated with piezoelectric composite layers under torsion loading

Jinquan Cheng *, Guoqiang Li

Department of Mechanical Engineering, Louisiana State University, Baton Rouge, LA 70803, USA

Received 2 January 2007; received in revised form 11 June 2007

Available online 21 December 2007

Abstract

In order to improve the joint failure strength, an adhesively bonded smart composite pipe joint system has been developed by integrating electromechanical coupling piezoelectric layers with the connection coupler. It has been validated that the integrated piezoelectric ceramic layers can smartly reduce stress concentration in the adhesive layer bond-line under bending or axial tension loads. In this study, piezoelectric particle/fiber reinforced polymer composite was utilized to construct adhesively bonded smart composite pipe joint systems, in order to overcome the brittle characteristic of the piezoelectric ceramic layers and to facilitate joint construction. Since torsion is one of the dominating loading conditions in practice, the behavior of the newly developed smart pipe joint system subjected to torsion loading was investigated in-detail to evaluate the effect of the integrated piezoelectric reinforced polymer composite layer on the joint performance. Firstly, based on the first-order shear deformation theory, the fundamental equations with relevant boundary and continuity conditions were developed to theoretically model the smart pipe joint system subjected to torsion loading. Further, the analytical solutions for the mid-plane displacements and the shear and peel stresses in the adhesive layer were obtained by using the Levy solution and the state-space method. Finally, some numerical examples were presented to evaluate the detailed effect of the stacking sequence and thickness of the integrated composite piezoelectric layers in the connection coupler on reducing the stress concentration in the adhesive layer; the effect of the applied electric fields on shear and peel stresses in the adhesive layer was also illustrated.

© 2007 Elsevier Ltd. All rights reserved.

Keywords: Smart structure; Pipe joint; Stress analysis; Piezoelectrics

1. Introduction

Due to their exceptional characteristics, such as lightweight, high strength to weight ratio and excellent corrosion-resistance, etc., fiber reinforced polymer composite materials are being utilized in an unprecedented rate in industry as more and more industrial sectors discover the benefits of these versatile materials in various structural components such as beam, plate, panel and pipe, etc. As is well-known, because of the limitation of

* Corresponding author.

E-mail address: hitejq@hotmail.com (J. Cheng).

manufacturing, transportation, and installation, a joint is an inevitable component to connect different structural components together for a large or integrated structure. Currently, joining methods can be roughly categorized into three main types: (1) mechanical fastening; (2) welding; and (3) adhesive bonding. Compared to the mechanical fastening and welding methods, there are several advantages associated with adhesively bonded joints, such as lower stress concentration, more uniform distribution of stress, lighter weight, water tightness, corrosion-resistance and better fatigue properties, especially for composite materials and structures. Recently with the advancement of adhesive material science and bonding techniques, a number of adhesively bonded joint systems have been increasingly used in engineering structures, such as single-lap joint, single-strap joint, double-lap joint and scarf joint in aeronautic, automotive and civil engineering structures. Corresponding to this general tendency, adhesively bonded composite piping systems have also been increasingly adopted in the marine, petrochemical and chemical industries. Composite piping has achieved an exclusive corrosion control and significant economic benefit in the world.

For any type of adhesively bonded joint systems, for instance beam/plate-like joint and tubular joint, the load transfer is always through the adhesive layer bond-line via peel and shear stresses. And, a significant peel/shear stress concentration always exists in the end region of the adhesive layer bond-line as verified by numerous previous theoretical and experimental works since 1944 (e.g. [Goland and Reissner, 1944](#); [Hart-Smith, 1973](#); [Adams and Wake, 1984](#) for the beam-like joint; and [Adams and Peppiatt, 1977](#); [Adams and Wake, 1984](#); [Chen and Cheng, 1992a,b](#) for the tubular joint). From the open literatures, it is seen that there are only a few studies reported for the tubular joint with comparison to the beam/plate-like joint, and the earlier theoretical analysis works were focused on the isotropic adherends. Recently, due to the broader and broader application of the composite piping system in various engineering fields, the composite pipe joint problem has attracted more and more attentions ([Graves and Adams, 1981](#); [Chon, 1982](#); [Hipol, 1984](#); [Hashim et al., 1998](#); [Yang, 2000](#); [Harte et al., 2003](#); [Yang et al., 2002](#); [Pugno and Carpinteri, 2003](#); [Kim and Lee, 2004](#); [Zou and Taheri, 2006](#); [Lees, 2006](#); [Cheng et al., 2006, 2007](#); [Oh, 2007](#)). Furthermore, most of the analyses were conducted to numerically obtain the basic stress distributions by the Finite Element Method (e.g. [Hashim et al., 1998](#); [Harte et al., 2003](#); [Kim and Lee, 2004](#)). There are only a few theoretical analyses conducted by the analytical solution methods in terms of the classical/first-order shear laminated plate/shell theory for torsion loading case. For example, [Zou and Taheri](#), based on the classical lamination theory, obtained a simple analytical solution ([Zou and Taheri, 2006](#)); [Oh](#) set up a first-order shear deformation theory-based model and used the stress-based solution method to study the nonlinear effect ([Oh, 2007](#)). From these previous works on the different types of joint systems, it was found that the peel/shear stress concentration in the end regions of the adhesive layer is the lethiferous reason for inducing premature failure of adhesively bonded joints. In order to prevent the joint systems from premature failure, how to reduce or even eliminate the stress concentration becomes a critical challenge for engineers and researchers. Up to now, some traditional and preventive enhancement methods have been successfully applied in engineering structures, including rounding off the sharp edges, spewing fillets and tapering of the adherends ([Hart-Smith, 1983](#); [Roberts, 1989](#); [Cheng et al., 1991](#)). Furthermore, some other mechanical stiffening methods have also been executed to improve the joint strength, such as using reinforcing patches to reduce the stress concentration in the adhesive layers ([Albat and Romilly, 1999](#)). Evidently, all of the above-mentioned strength enhancement methods are the traditional geometric improvement or mechanical stiffening ones which belong to the passive method for improving the joint strength capacity. They are unable to adaptively survive sudden and unexpected loadings. Thus, in order to enhance the survivability of a joint system, it is desired to develop an adaptive adhesively bonded joint system for better serving the working environment.

Considering the fact that smart materials can act as sensors and actuators in engineering structures, [Cheng and Taheri et al.](#) have firstly introduced a smart material – a high performance electro-mechanical coupling piezoelectrics into the adhesively bonded beam-like joint system to realize the adaptive strength enhancement by the external electric field ([Cheng and Taheri, 2005, 2006](#); [Cheng et al., 2006](#)). Further, the adhesively bonded smart composite pipe joint systems were also developed and analyzed to verify the smart effect of the integrated piezoelectric layers on the pipe joint strength improvement when the pipe joint system was subjected to an axial tension load or a bending load ([Cheng et al., 2006, 2007](#)). However, the well-known brittle characteristic of the piezoelectric ceramics has limited their extensive application in engineering structures, particularly for structures with complicated construction, larger deformation and vibration. Compared to

the general brittle piezoelectric ceramics, the advantages of piezoelectric particle/fiber reinforced composites with flexible matrix have attracted attentions of many researchers (Wang, 1992; Cheng et al., 2000; Jiang and Batra, 2001; Tan and Tong, 2001; Wu et al., 2001; Włodzimierz and Przybyłowicz, 2003; Cheng et al., 2005a,b). These piezoelectric composites have been successfully utilized as actuators/sensors to control/monitor large static deformation and dynamic vibration of various complicated large structures (Włodzimierz and Przybyłowicz, 2003; Cheng et al., 2005a,b). Thus, without loss of generality, we can extend the application of the flexible piezoelectric fiber/particle reinforced polymer composite to fabricate the new connection coupler for the pipe joint.

It is well known that torsion load is another representative loading case in practice, in addition to the bending load and axial tension load. Therefore based on the previous works, we focused on studying the detailed effect of the integrated piezoelectric reinforced composite layer on the behavior of an adhesively bonded smart composite pipe joint system subjected to a torsion loading at the joint end in this paper. In order to verify the developed smart pipe joint system, a theoretical model was set up by using the first-order shear deformation theory to obtain fundamental expressions for the joint system by considering the electro-mechanical coupling effect of the integrated piezoelectric reinforced composite layers in the connection coupler. Here, the effective electro-elastic properties of piezoelectric reinforced composite materials were predicted by the micromechanical Mori–Tanaka's electromechanical method. Then, considering the geometric symmetry characteristics, the Levy-type-based solution method was employed to obtain the basic solution for the governing equations based on the relevant boundary/continuity conditions when the joint was subjected to a torsion loading at the joint end. Further, the state-space method was utilized to obtain the final analytical solutions, including the peel and shear stress distributions in the adhesive layer bond-line. Finally, some detailed numerical simulations were conducted to demonstrate the design and optimization of the smart composite pipe joint system under the combined torsion loading and electric fields, including the thickness and stacking sequence of the integrated piezoelectric reinforced composite layers in the connection coupler.

2. Basic structure and fundamental equations

2.1. Basic structure

As is well-known, an adhesively bonded pipe joint system is generally composed of two pieces of pipes, a connection coupler and an adhesive layer, such as a single-strap type pipe joint, as shown in Fig. 1. Previously, we have studied the performance enhancement of this type of joints by integrating piezoelectric ceramic layers when the joint is subjected to an axial tension load or a bending load (Cheng et al., 2006, 2007). Based on the above discussion, piezoelectric particle/fiber reinforced polymer composite layer will be used instead of piezoelectric ceramic layers in this study because the piezoelectric composite is more ductile or flexible to meet with the requirement for higher ductility in the connection coupler. A schematic of the piezoelectric particle/fiber reinforced polymer composite is shown in Fig. 2. A sectional view of a single-strap pipe joint integrated with the piezoelectric composite layer is schematically shown in Fig. 3. In the next sections, the detailed theoretical modeling and analyses will be carried out for verifying the developed smart joint system shown in Fig. 3.

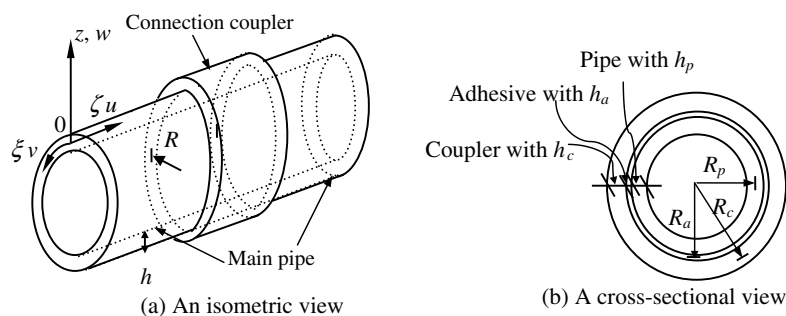


Fig. 1. A schematic geometric view of the pipe joint.

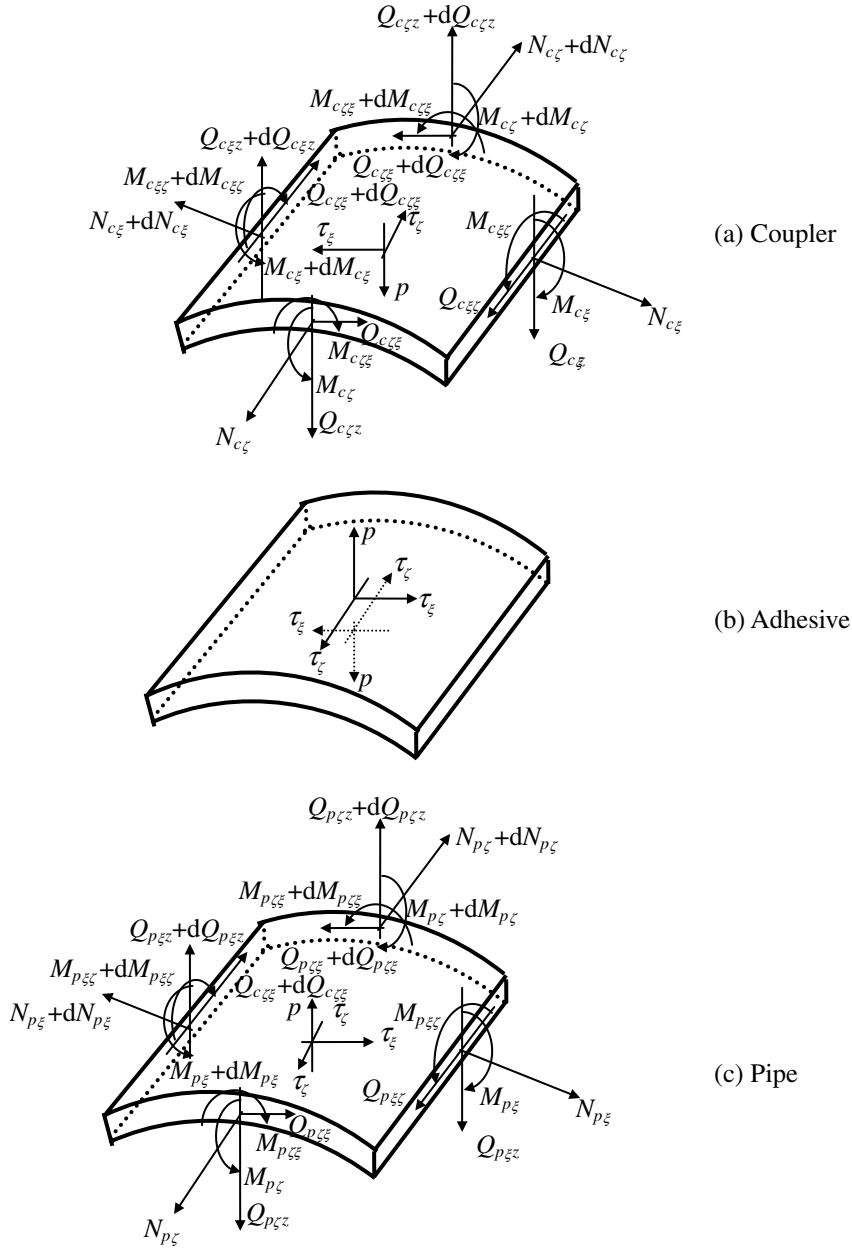


Fig. 5. The stresses and forces on the infinitesimal element of a joint system: (a) the top layer (connection coupler), (b) the adhesive layer and (c) the bottom layer (main pipe).

$$\frac{\partial N_{b\zeta}}{\partial \zeta} + \frac{\partial Q_{b\zeta\zeta}}{\partial \zeta_p} = 0 \quad (1a)$$

$$\frac{\partial N_{b\zeta}}{\partial \zeta_b} + \frac{Q_{b\zeta\zeta}}{R_p} + \frac{\partial Q_{b\zeta\zeta}}{\partial \zeta} = 0 \quad (1b)$$

$$\frac{\partial Q_{b\zeta\zeta}}{\partial \zeta} + \frac{\partial Q_{b\zeta\zeta}}{\partial \zeta_p} - \frac{N_{b\zeta}}{R_p} = 0 \quad (1c)$$

$$\frac{\partial M_{b\zeta}}{\partial \zeta} - Q_{b\zeta} + \frac{\partial M_{b\zeta\zeta}}{\partial \zeta_p} = 0 \quad (1d)$$

$$\frac{\partial M_{b\zeta}}{\partial \zeta_p} - Q_{b\zeta} + \frac{\partial M_{b\zeta\zeta}}{\partial \zeta} = 0 \quad (1e)$$

For the pipe part covered by the connection coupler, the following equilibrium equations in the local coordinate system can be obtained by considering the effect of the adhesive layer stresses:

$$\frac{\partial N_{p\zeta}}{\partial \zeta} + \frac{\partial Q_{p\zeta\zeta}}{\partial \zeta_p} = \frac{R_{po}}{R_p} \tau_\zeta \quad (2a)$$

$$\frac{\partial N_{p\zeta}}{\partial \zeta_p} + \frac{Q_{p\zeta}}{R_p} + \frac{\partial Q_{p\zeta\zeta}}{\partial \zeta} = \frac{R_{po}}{R_p} \tau_\zeta \quad (2b)$$

$$\frac{\partial Q_{p\zeta}}{\partial \zeta} + \frac{\partial Q_{p\zeta\zeta}}{\partial \zeta_p} - \frac{N_{p\zeta}}{R_p} = -\frac{R_{po}}{R_p} p \quad (2c)$$

$$\frac{\partial M_{p\zeta}}{\partial \zeta} - Q_{p\zeta} + \frac{\partial M_{p\zeta\zeta}}{\partial \zeta_p} = \frac{h_p}{2} \frac{R_{po}}{R_p} \tau_\zeta \quad (2d)$$

$$\frac{\partial M_{p\zeta}}{\partial \zeta_p} - Q_{p\zeta} + \frac{\partial M_{p\zeta\zeta}}{\partial \zeta} = \frac{h_p}{2} \frac{R_{po}}{R_p} \tau_\zeta \quad (2e)$$

And in the connection coupler, the equilibrium equations can be described in the local coordinate system by:

$$\frac{\partial N_{c\zeta}}{\partial \zeta} + \frac{\partial Q_{c\zeta\zeta}}{\partial \zeta_c} = -\frac{R_{ci}}{R_c} \tau_\zeta \quad (3a)$$

$$\frac{\partial N_{c\zeta}}{\partial \zeta_c} + \frac{Q_{c\zeta}}{R_c} + \frac{\partial Q_{c\zeta\zeta}}{\partial \zeta} = -\frac{R_{ci}}{R_c} \tau_\zeta \quad (3b)$$

$$\frac{\partial Q_{c\zeta}}{\partial \zeta} + \frac{\partial Q_{c\zeta\zeta}}{\partial \zeta_c} - \frac{N_{c\zeta}}{R_c} = \frac{R_{ci}}{R_c} p \quad (3c)$$

$$\frac{\partial M_{c\zeta}}{\partial \zeta} - Q_{c\zeta} + \frac{\partial M_{c\zeta\zeta}}{\partial \zeta_c} = \frac{h_c}{2} \frac{R_{ci}}{R_c} \tau_\zeta \quad (3d)$$

$$\frac{\partial M_{c\zeta}}{\partial \zeta_c} - Q_{c\zeta} + \frac{\partial M_{c\zeta\zeta}}{\partial \zeta} = \frac{h_c}{2} \frac{R_{ci}}{R_c} \tau_\zeta \quad (3e)$$

Here the subscripts “p, b, c” of the resulting forces and moments denote the overlapped main pipe part, bare main pipe and connection coupler, respectively. R_a is the radius of the adhesive layer and $R_a = \frac{R_{ci} + R_{po}}{2}$. R_{ci} and R_{po} are the inner radius of the connection coupler and the outer radius of the main pipe, i.e. the top and bottom surfaces of the adhesive layer, respectively. Based on the first-order deformation theory for laminated composite structures, the resulting forces $N_{i\zeta}$, $N_{i\zeta}$, $Q_{i\zeta\zeta}$, $Q_{i\zeta\zeta}$, $Q_{i\zeta\zeta}$ and $Q_{i\zeta\zeta}$, and, moments $M_{i\zeta}$, $M_{i\zeta}$, $M_{i\zeta\zeta}$ and $M_{i\zeta\zeta}$ ($i = p, b, c$) for the different sections can be obtained by

$$\begin{aligned} N_{i\zeta} &= N_{i11} = \int_{-\frac{h_i}{2}}^{\frac{h_i}{2}} \frac{(R_i + z)}{R_i} \sigma_1 dz = \sum_{k=1}^n \int_{z_k}^{z_{k+1}} \frac{(R_i + z)}{R_i} (\bar{Q}_{11}^k \varepsilon_1 + \bar{Q}_{12}^k \varepsilon_2 - \bar{e}_{31}^k E_3^k) dz \\ &= A_{i11} \frac{\partial u_{i0}}{\partial \zeta} + B_{i11} \frac{\partial \phi_i}{\partial \zeta} + \frac{1}{R_i} A_{i12} w_i + A_{i12} \frac{\partial v_{i0}}{\partial \zeta_i} + B_{i12} \frac{\partial \phi_i}{\partial \zeta_i} - N_{i\zeta}^{PZT} \end{aligned} \quad (4a)$$

$$\begin{aligned} N_{i\zeta} &= N_{i22} = \int_{-\frac{h_i}{2}}^{\frac{h_i}{2}} \sigma_2 dz = \sum_{k=1}^n \int_{z_k}^{z_{k+1}} (\bar{Q}_{21}^k \varepsilon_1 + \bar{Q}_{22}^k \varepsilon_2 - \bar{e}_{32}^k E_3^k) dz \\ &= A_{i21} \frac{\partial u_{i0}}{\partial \zeta} + B_{i21} \frac{\partial \phi_i}{\partial \zeta} + \frac{1}{R_i} A_{i22} w_i + A_{i22} \frac{\partial v_{i0}}{\partial \zeta_i} + B_{i22} \frac{\partial \phi_i}{\partial \zeta_i} - N_{i\zeta}^{PZT} \end{aligned} \quad (4b)$$

$$\begin{aligned}
M_{i\zeta} &= M_{i11} = \int_{-\frac{h_i}{2}}^{\frac{h_i}{2}} \frac{(R_i + z)}{R_i} \sigma_1 z \, dz = \sum_{k=1}^n \int_{z_k}^{z_{k+1}} \frac{(R_i + z)}{R_i} (\bar{Q}_{11}^k \varepsilon_1 + \bar{Q}_{12}^k \varepsilon_2 - \bar{e}_{31}^k E_3^k) z \, dz \\
&= B_{i11} \frac{\partial u_{i0}}{\partial \zeta} + D_{i11} \frac{\partial \phi_i}{\partial \zeta} + \frac{1}{R_i} B_{i12} w_i + B_{i12} \frac{\partial v_{i0}}{\partial \zeta_i} + D_{i12} \frac{\partial \varphi_i}{\partial \zeta_i} - M_{i\zeta}^{\text{PZT}}
\end{aligned} \quad (4c)$$

$$\begin{aligned}
M_{i\zeta} &= M_{i22} = \int_{-\frac{h_i}{2}}^{\frac{h_i}{2}} \sigma_2 z \, dz = \sum_{k=1}^n \int_{z_k}^{z_{k+1}} (\bar{Q}_{21}^k \varepsilon_1 + \bar{Q}_{22}^k \varepsilon_2 - \bar{e}_{32}^k E_3^k) z \, dz \\
&= B_{i21} \frac{\partial u_{i0}}{\partial \zeta} + D_{i21} \frac{\partial \phi_i}{\partial \zeta} + \frac{1}{R_i} B_{i22} w_i + B_{i22} \frac{\partial v_{i0}}{\partial \zeta_i} + D_{i22} \frac{\partial \varphi_i}{\partial \zeta_i} - M_{i\zeta}^{\text{PZT}}
\end{aligned} \quad (4d)$$

$$\begin{aligned}
M_{i\zeta\zeta} &= M_{i12} = \int_{-\frac{h_i}{2}}^{\frac{h_i}{2}} \frac{(R_i + z)}{R_i} \sigma_6 z \, dz = \sum_{k=1}^n \int_{z_k}^{z_{k+1}} \frac{(R_i + z)}{R_i} \bar{Q}_{66}^k \varepsilon_6 z \, dz \\
&= B_{i661} \frac{\partial u_{i0}}{\partial \zeta_i} + D_{i661} \frac{\partial \phi_i}{\partial \zeta_i} + \left(B_{i661} + \frac{1}{R_i} D_{i661} \right) \frac{\partial v_{i0}}{\partial \zeta} + \left(D_{i661} + \frac{1}{R_i} E_{i661} \right) \frac{\partial \varphi_i}{\partial \zeta}
\end{aligned} \quad (4e)$$

$$M_{i\zeta\zeta} = M_{i21} = \int_{-\frac{h_i}{2}}^{\frac{h_i}{2}} \sigma_6 z \, dz = \sum_{k=1}^n \int_{z_k}^{z_{k+1}} \bar{Q}_{66}^k \varepsilon_6 z \, dz = B_{i662} \frac{\partial u_{i0}}{\partial \zeta_i} + D_{i662} \frac{\partial \phi_i}{\partial \zeta_i} + B_{i661} \frac{\partial v_{i0}}{\partial \zeta} + D_{i661} \frac{\partial \varphi_i}{\partial \zeta} \quad (4f)$$

$$\begin{aligned}
Q_{i\zeta\zeta} &= Q_{i12} = \int_{-\frac{h_i}{2}}^{\frac{h_i}{2}} \frac{R_i + z}{R_i} \sigma_6 \, dz = \sum_{k=1}^n \int_{z_k}^{z_{k+1}} \frac{R_i + z}{R_i} \bar{Q}_{66}^k \varepsilon_6 \, dz \\
&= A_{i661} \frac{\partial u_{i0}}{\partial \zeta_i} + B_{i661} \frac{\partial \phi_i}{\partial \zeta_i} + \left(A_{i661} + \frac{1}{R_i} B_{i661} \right) \frac{\partial v_{i0}}{\partial \zeta} + \left(B_{i661} + \frac{1}{R_i} D_{i661} \right) \frac{\partial \varphi_i}{\partial \zeta}
\end{aligned} \quad (4g)$$

$$Q_{i\zeta\zeta} = Q_{i21} = \int_{-\frac{h_i}{2}}^{\frac{h_i}{2}} \sigma_6 \, dz = \sum_{k=1}^n \int_{z_k}^{z_{k+1}} \bar{Q}_{66}^k \varepsilon_6 \, dz = A_{i662} \frac{\partial u_{i0}}{\partial \zeta_i} + B_{i662} \frac{\partial \phi_i}{\partial \zeta_i} + A_{i661} \frac{\partial v_{i0}}{\partial \zeta} + B_{i661} \frac{\partial \varphi_i}{\partial \zeta} \quad (4h)$$

$$Q_{i\zeta z} = Q_{iz\zeta} = Q_{i23} = Q_{i32} = \int_{-\frac{h_i}{2}}^{\frac{h_i}{2}} \sigma_4 \, dz = \sum_{k=1}^n \int_{z_k}^{z_{k+1}} K \bar{Q}_{44}^k \varepsilon_4 \, dz = A_{i44} \frac{\partial w_i}{\partial \zeta_i} - \frac{1}{R_i} A_{i44} v_{i0} + A_{i44} \varphi_i \quad (4i)$$

$$Q_{iz\zeta} = Q_{i\zeta z} = Q_{i31} = Q_{i13} = \int_{-\frac{h_i}{2}}^{\frac{h_i}{2}} \frac{(R_i + z)}{R_i} \sigma_5 \, dz = \sum_{k=1}^n \int_{z_k}^{z_{k+1}} \frac{(R_i + z)}{R_i} K \bar{Q}_{55}^k \varepsilon_5 \, dz = A_{i55} \phi_i + A_{i55} \frac{\partial w_{i0}}{\partial \zeta} \quad (4j)$$

where these resultant forces and moments are general expressions for any parts of pipe joint system, i.e. $i = p, b$ or c . For instance, the above resultant forces and moments will represent the resultant forces and moments of the pipe if the radius R in the general expressions is replaced by R_p . In the same manner, the resultant forces and moments for other parts can be obtained. The shell stiffnesses are re-defined and used in the above derivation, i.e. $A_{\text{inn}}, B_{\text{inn}}$, etc.

The additional resultant forces N_{ij}^{PZT} and moments M_{ij}^{PZT} ($i = j = 1, 2$) are caused by external electric fields that are applied to the integrated piezoelectric reinforced composite layers in the connection coupler as defined by:

$$N_{c\zeta}^{\text{PZT}} = N_{c11}^{\text{PZT}} = \sum_{k=1}^n \int_{z_k}^{z_{k+1}} \frac{(R_c + z)}{R_c} \bar{e}_{31}^k E_3^k dz \quad (5a)$$

$$N_{c\xi}^{\text{PZT}} = N_{c22}^{\text{PZT}} = \sum_{k=1}^n \int_{z_k}^{z_{k+1}} \bar{e}_{32}^k E_3^k dz \quad (5b)$$

$$M_{c\zeta}^{\text{PZT}} = M_{c11}^{\text{PZT}} = \sum_{k=1}^n \int_{z_k}^{z_{k+1}} \frac{(R_c + z)}{R_c} \bar{e}_{31}^k E_3^k z dz \quad (5c)$$

$$M_{c\xi}^{\text{PZT}} = M_{c22}^{\text{PZT}} = \sum_{k=1}^n \int_{z_k}^{z_{k+1}} z \bar{e}_{32}^k E_3^k dz \quad (5d)$$

with the electric field applied to the distribution covered surface electrode represented by a 2D Heaviside Step function $H(x - x_0)$ (detailed definition for the piezoelectric partially covered electrode can be found in Lee and Moon's paper (Lee and Moon, 1990)), as:

$$E_3^k(\zeta, \xi) = E_{30}^k [H(\zeta - \zeta_0) - H(\zeta - \zeta_1)] \times [H(\xi - \xi_0) - H(\xi - \xi_1)] \quad (6)$$

where \bar{e}_{ij}^k is the piezo-coefficients of the piezoelectric reinforced composite materials, and determined by the effective electro-elastic properties of piezoelectric reinforced composite that were predicted by the developed micromechanical Mori–Tanaka's electromechanical method as given in Appendix A.

Furthermore, τ_ζ , τ_ξ and p denote the shear and normal (peel) stresses in the adhesive layer in the ζ -axis, ξ -axis and z -axis as shown in Fig. 5b, respectively. Evidently, the shear and normal stresses in the adhesive layer are caused by the discontinuity of the relative displacements on the top and bottom surfaces of the adhesive layer. Assuming that the adhesive shear stresses are uniform throughout the thickness of the adhesive layer, the shear stresses τ_ζ and τ_ξ can be obtained from the above assumed displacement fields of the pipe and coupler by using the average values of $\frac{\partial w_c}{\partial \zeta}$, $\frac{\partial w_p}{\partial \zeta}$, $\frac{\partial w_c}{\partial \xi}$ and $\frac{\partial w_p}{\partial \xi}$ in the following forms:

$$\tau_\zeta = G_a \left(\frac{u_p - u_c}{h_a} \right) - \frac{G_a}{2} \left(\frac{\partial w_c}{\partial \zeta} + \frac{\partial w_p}{\partial \zeta} \right) = G_a \left(\frac{u_{p0} - u_{c0}}{h_a} + \frac{\phi_p h_p + \phi_c h_c}{2h_a} \right) - \frac{G_a}{2} \left(\frac{\partial w_c}{\partial \zeta} + \frac{\partial w_p}{\partial \zeta} \right) \quad (7a)$$

$$\begin{aligned} \tau_\xi &= G_a \left(\frac{v_p - v_c}{h_a} \right) - \frac{G_a}{2} \left(\frac{\partial w_p}{\partial \xi} + \frac{\partial w_c}{\partial \xi} \right) + \frac{G_a}{2} \left(\frac{v_p + v_c}{R_a} \right) \\ &= G_a \left(\frac{v_{p0} - v_{c0}}{h_a} + \frac{v_{p0} + v_{c0}}{2R_a} + \frac{\phi_p h_p + \phi_c h_c}{2h_a} + \frac{\phi_p h_p - \phi_c h_c}{4R_a} \right) - \frac{G_a}{2} \left(\frac{\partial w_p}{\partial \xi} + \frac{\partial w_c}{\partial \xi} \right) \end{aligned} \quad (7b)$$

In the same manner, the normal stress p of the adhesive layer can be determined from the relative radial displacements of the pipe and coupler:

$$\begin{aligned} p &= \frac{E_a}{(1 + v_a)(1 - 2v_a)} \left[(1 - v_a) \left(\frac{w_c - w_p}{h_a} \right) + v_a \left(\frac{\epsilon_{p\zeta} + \epsilon_{c\zeta}}{2} \right) + v_a \left(\frac{\epsilon_{p\xi} + \epsilon_{c\xi}}{2} \right) \right] \\ &= \frac{E_a}{(1 + v_a)(1 - 2v_a)} \left\{ (1 - v_a) \left(\frac{w_c - w_p}{h_a} \right) + \frac{v_a}{2} \left(\frac{\partial u_{p0}}{\partial \zeta} + \frac{h_p}{2} \frac{\partial \phi_p}{\partial \zeta} + \frac{\partial u_{c0}}{\partial \zeta} - \frac{h_c}{2} \frac{\partial \phi_c}{\partial \zeta} \right) \right. \\ &\quad \left. + \frac{v_a}{2} \left[\frac{w_p}{R_{p0}} + \frac{R_p}{R_{p0}} \left(\frac{\partial v_{p0}}{\partial \xi} + \frac{h_p}{2} \frac{\partial \phi_p}{\partial \xi} \right) + \frac{w_c}{R_{ci}} + \frac{R_c}{R_{ci}} \left(\frac{\partial v_{c0}}{\partial \xi} - \frac{h_c}{2} \frac{\partial \phi_c}{\partial \xi} \right) \right] \right\} \end{aligned} \quad (7c)$$

where G_a , E_a and v_a are the shear modulus, Young's modulus and Poisson's ratio of the adhesive, respectively. h_a is the thickness of the adhesive layer.

2.3. Boundary and continuity conditions for a pipe joint subjected to torsion loading at the joint end

In order to solve the governing equations as presented above, the complement boundary/continuity conditions are required. In this paper, we mainly focused on the torsion loading case, i.e., the symmetric composite pipe joint system that is subjected to the torsion loading T , as shown in Fig. 4. It is generally assumed that the torsion loading is a linearly varying shear stress through the thickness with its force resultant equivalent to the

value of $Q_{b\zeta\zeta}$ as defined in Eq. (4) in the shell theory. Then, the shear stress along the thickness can be obtained as follows:

$$\sigma_{b\zeta\zeta} = \frac{2\rho T}{\left(R_{rpo}^4 - R_{rpi}^4\right)}, \quad R_{rpi} < \rho < R_{rpo} \quad (8)$$

Further, the related resultant force $\tilde{Q}_{b\zeta\zeta}$ and moment $\tilde{M}_{b\zeta\zeta}$ applied to the shell can be calculated in terms of the definitions in Eqs. (4) and (8), which are the prescribed boundary conditions at the joint end caused by the external torsion loading.

Therefore, for a joint system subjected to a torsion loading, the relevant boundary and continuity conditions about the forces/moments and displacements can be described for different parts of the system detailed as follows:

$$\text{At } x_2 = l_2 : \quad N_{b\zeta} = 0, \quad Q_{b\zeta\zeta} = \tilde{Q}_{b\zeta\zeta}, \quad Q_{b\zeta z} = 0, \quad M_{b\zeta} = 0, \quad M_{b\zeta\zeta} = \tilde{M}_{b\zeta\zeta} \quad (9a)$$

$$\text{At } x_1 = l_1 : \quad N_{c\zeta} = 0, \quad Q_{c\zeta\zeta} = 0, \quad Q_{c\zeta z} = 0, \quad M_{c\zeta} = 0, \quad M_{c\zeta\zeta} = 0 \quad (9b)$$

$$\text{At } x_1 = 0 : \quad N_{p\zeta} = 0, \quad Q_{p\zeta\zeta} = 0, \quad Q_{p\zeta z} = 0, \quad M_{p\zeta} = 0, \quad M_{p\zeta\zeta} = 0 \quad (9c)$$

$$u_{0c} = 0, \quad \phi_c = 0, \quad v_{0c} = 0, \quad \varphi_c = 0, \quad w_c = 0 \quad (9d)$$

$$\text{At } x_1 = l_1 \text{ and } x_2 = 0 : \quad N_{p\zeta} = N_{b\zeta}, \quad Q_{p\zeta\zeta} = Q_{b\zeta\zeta}, \quad Q_{p\zeta z} = Q_{b\zeta z}, \quad M_{p\zeta} = M_{b\zeta}, \quad M_{p\zeta\zeta} = M_{b\zeta\zeta}, \quad (9e)$$

$$u_{0p} = u_{0b}, \quad \phi_p = \phi_b, \quad v_{0p} = v_{0b}, \quad \varphi_p = \varphi_b, \quad w_p = w_b \quad (9f)$$

where the upper “~” of the above variables denotes the prescribed external forces and moments. It is seen that there are a total of 30 boundary and continuity conditions for the problem, which insures that the present problem solution is close.

2.4. Displacement-based governing equation

The displacement-based governing equations for the different parts of the composite pipe joint system can be obtained by plugging the resultant forces and moments Eq. (4) and the strain–displacement relationships into the above equilibrium equations. For example, in the coupled pipe part, the displacement-based governing equations can be expressed in the local coordinate system as

$$\begin{aligned} & A_{p11} \frac{\partial^2 u_{p0}}{\partial \zeta^2} + B_{p11} \frac{\partial^2 \phi_p}{\partial \zeta^2} + \frac{1}{R_p} A_{p12} \frac{\partial w_p}{\partial \zeta} + (A_{p12} + A_{p661}) \frac{\partial^2 v_{p0}}{\partial \zeta_p \partial \zeta} + (B_{p12} + B_{p661}) \frac{\partial^2 \varphi_p}{\partial \zeta_p \partial \zeta} + A_{p662} \frac{\partial^2 u_{p0}}{\partial \zeta_p^2} + B_{p662} \frac{\partial^2 \phi_p}{\partial \zeta_p^2} \\ & = \frac{R_{po}}{R_p} \left[G_a \left(\frac{u_{p0} - u_{c0}}{h_a} + \frac{h_p \phi_p + h_c \phi_c}{2h_a} \right) - \frac{G_a}{2} \left(\frac{\partial w_c}{\partial \zeta} + \frac{\partial w_p}{\partial \zeta} \right) \right] \end{aligned} \quad (10a)$$

$$\begin{aligned} & (A_{p21} + A_{p662}) \frac{\partial^2 u_{p0}}{\partial \zeta \partial \zeta_p} + (B_{p21} + B_{p662}) \frac{\partial^2 \phi_p}{\partial \zeta \partial \zeta_p} + \frac{1}{R_p} (A_{p22} + A_{p44}) \frac{\partial w_p}{\partial \zeta_p} + A_{p22} \frac{\partial^2 v_{p0}}{\partial \zeta_p^2} + B_{p22} \frac{\partial^2 \varphi_p}{\partial \zeta_p^2} \\ & + \frac{1}{R_p} \left(-\frac{1}{R_p} A_{p44} v_{p0} + A_{p44} \varphi_p \right) + A_{p661} \frac{\partial^2 v_{p0}}{\partial \zeta^2} + B_{p661} \frac{\partial^2 \varphi_p}{\partial \zeta^2} = \frac{R_{po}}{R_p} \left[G_a \left(\frac{v_{p0} - v_{c0}}{h_a} + \frac{h_p \varphi_p + h_c \varphi_c}{2h_a} \right) \right. \\ & \left. - \frac{G_a}{2} \left(\frac{\partial w_p}{\partial \zeta_p} + \frac{\partial w_c}{\partial \zeta_c} \right) + \frac{G_a}{2} \left(\frac{v_{p0} + v_{c0}}{R_a} + \frac{h_p \varphi_p - h_c \varphi_c}{2R_a} \right) \right] \end{aligned} \quad (10b)$$

$$\begin{aligned} & (A_{p55} - \frac{1}{R_p} B_{p21}) \frac{\partial \phi_p}{\partial \zeta} + A_{p55} \frac{\partial^2 w_p}{\partial \zeta^2} + A_{p44} \frac{\partial^2 w_p}{\partial \zeta_p^2} - \frac{1}{R_p} (A_{p44} + A_{p22}) \frac{\partial v_{p0}}{\partial \zeta_p} + (A_{p44} - \frac{1}{R_p} B_{p22}) \frac{\partial \varphi_p}{\partial \zeta_p} \\ & - \frac{1}{R_p} \left(A_{p21} \frac{\partial u_{p0}}{\partial \zeta} + \frac{1}{R_p} A_{p22} w_p \right) = -\frac{R_{po}}{R_p} \frac{E_a}{(1 + v_a)(1 - 2v_a)} \left\{ (1 - v_a) \frac{w_c - w_p}{h_a} + \frac{v_a}{2} \left(\frac{\partial u_{p0}}{\partial \zeta} + \frac{h_p}{2} \frac{\partial \phi_p}{\partial \zeta} \right) \right. \\ & \left. + \frac{\partial u_{c0}}{\partial \zeta} - \frac{h_c}{2} \frac{\partial \phi_c}{\partial \zeta} \right\} + \frac{v_a}{2} \left[\frac{w_p}{R_{po}} + \frac{R_p}{R_{po}} \left(\frac{\partial v_{p0}}{\partial \zeta_p} + \frac{h_p}{2} \frac{\partial \varphi_p}{\partial \zeta_p} \right) + \frac{w_c}{R_{ci}} + \frac{R_c}{R_{ci}} \left(\frac{\partial v_{c0}}{\partial \zeta_c} - \frac{h_c}{2} \frac{\partial \varphi_c}{\partial \zeta_c} \right) \right] \end{aligned} \quad (10c)$$

$$B_{p11} \frac{\partial^2 u_{p0}}{\partial \zeta^2} + D_{p11} \frac{\partial^2 \phi_p}{\partial \zeta^2} + \left(\frac{1}{R_p} B_{p12} - A_{p55} \right) \frac{\partial w_p}{\partial \zeta} + (B_{p12} + B_{p661}) \frac{\partial^2 v_{p0}}{\partial \zeta_p \partial \zeta} + (D_{p12} + D_{p661}) \frac{\partial^2 \phi_p}{\partial \zeta_p \partial \zeta} - A_{p55} \phi_p$$

$$+ B_{p662} \frac{\partial^2 u_{p0}}{\partial \zeta_p^2} + D_{p662} \frac{\partial^2 \phi_p}{\partial \zeta_p^2} = \frac{h_p}{2} \frac{R_{p0}}{R_p} \left[G_a \left(\frac{u_{p0} - u_{c0}}{h_a} + \frac{h_p \phi_p + h_c \phi_c}{2h_a} \right) - \frac{G_a}{2} \left(\frac{\partial w_c}{\partial \zeta} + \frac{\partial w_p}{\partial \zeta} \right) \right] \quad (10d)$$

$$(B_{p21} + B_{p661}) \frac{\partial^2 u_{p0}}{\partial \zeta \partial \zeta_p} + (D_{p21} + D_{p661}) \frac{\partial^2 \phi_p}{\partial \zeta \partial \zeta_p} + \left(\frac{1}{R_p} B_{p22} - A_{p44} \right) \frac{\partial w_p}{\partial \zeta_p} + B_{p22} \frac{\partial^2 v_{p0}}{\partial \zeta_p^2} + D_{p22} \frac{\partial^2 \phi_p}{\partial \zeta_p^2}$$

$$- \left(-\frac{1}{R_p} A_{p44} v_{p0} + A_{p44} \phi_p \right) + \left(B_{p661} + \frac{1}{R_p} D_{p661} \right) \frac{\partial^2 v_{p0}}{\partial \zeta^2} + \left(D_{p661} + \frac{1}{R_p} E_{p661} \right) \frac{\partial^2 \phi_p}{\partial \zeta^2}$$

$$= \frac{h_p}{2} \frac{R_{p0}}{R_p} \left[G_a \left(\frac{v_{p0} - v_{c0}}{h_a} + \frac{h_p \phi_p + h_c \phi_c}{2h_a} \right) - \frac{G_a}{2} \left(\frac{\partial w_p}{\partial \zeta_p} + \frac{\partial w_c}{\partial \zeta_c} \right) + \frac{G_a}{2} \left(\frac{v_{p0} + v_{c0}}{R_a} + \frac{h_p \phi_p - h_c \phi_c}{2R_a} \right) \right] \quad (10e)$$

Similarly, the displacement-based governing equations for the bare pipe part and connection coupler part can also be obtained in the respective local coordinate systems.

Evidently, based on the above governing equation analyses, there are a total of 15 second-order differential equations with 15 unknown variables, i.e. u_{p0} , ϕ_p , v_{p0} , ϕ_p and w_p in the coupled pipe part, u_{b0} , ϕ_b , v_{b0} , ϕ_b and w_b in the bare pipe part, u_{c0} , ϕ_c , v_{c0} , ϕ_c and w_c in the connection coupler part for final determination. Thus, it requires 30 complement boundary/continuity conditions of the overall joint system for the complete closed-form solution; see Eq. (9). In order to obtain the analytical solutions for these differential equations, a coordinate transform is introduced to transform the above differential equations into a uniform coordinate system as follows:

$$\frac{\xi_a}{\xi_p} = \frac{R_a}{R_p} \quad \text{and} \quad \frac{\xi_a}{\xi_c} = \frac{R_a}{R_c} \quad (11)$$

Further some coordinate transform relationships can be represented by:

$$\frac{\partial(\cdot)}{\partial \xi_p} = \frac{R_a}{R_p} \frac{\partial(\cdot)}{\partial \xi_a}, \quad \frac{\partial^2(\cdot)}{\partial \xi_p^2} = \left(\frac{R_a}{R_p} \right)^2 \frac{\partial^2(\cdot)}{\partial \xi_a^2}, \quad \frac{\partial(\cdot)}{\partial \xi_c} = \frac{R_a}{R_c} \frac{\partial(\cdot)}{\partial \xi_a}, \quad \frac{\partial^2(\cdot)}{\partial \xi_c^2} = \left(\frac{R_a}{R_c} \right)^2 \frac{\partial^2(\cdot)}{\partial \xi_a^2}$$

where the notation ‘ \cdot ’ inside the bracket denotes the differential variables. After applying the above coordinate transforms to the displacement-based governing equations and the relevant boundary and continuity conditions for the three parts in their respective local coordinate system, a new set of governing equations with 15 unknown variables and 30 relevant boundary and continuity conditions can be represented in the uniform coordinate system.

3. Analytical solution procedure

Based on the previous works about the Levy-based solution procedure for a circular cylindrical shell with arbitrary boundary conditions at the end (Whitney, 1987; Reddy, 2004), we can express the generalized displacements (u_0 , ϕ , v_0 , ϕ and w) as products of unknown functions and known trigonometric functions of spatial coordinates for arbitrary combinations of free, clamped and simply-supported boundary conditions. Thus, considering the symmetry, anti-symmetry and continuity of the circular geometry and applied loading, the general solutions by the Fourier series in the ξ_a -axis can be expressed as

$$u_0(\varsigma, \xi) = \sum_n U(\varsigma) \cos \left(\frac{n \xi_a}{R_a} \right), \quad \phi(\varsigma, \xi) = \sum_n \Phi(\varsigma) \cos \left(\frac{n \xi_a}{R_a} \right) \quad (12a)$$

$$v_0(\varsigma, \xi) = \sum_n V(\varsigma) \sin \left(\frac{n \xi_a}{R_a} \right), \quad \phi(\varsigma, \xi) = \sum_n \Psi(\varsigma) \sin \left(\frac{n \xi_a}{R_a} \right) \quad (12b)$$

$$w(\varsigma, \xi) = \sum_n W(\varsigma) \cos \left(\frac{n \xi_a}{R_a} \right) \quad (12c)$$

It is noted that the above basic solutions are general solutions and suitable for the three different parts of the joint. So far, 15 new unknown variables, $U_p(\zeta)$, $\Phi_p(\zeta)$, $V_p(\zeta)$, $\Psi_p(\zeta)$, $W_p(\zeta)$, $U_b(\zeta)$, $\Phi_b(\zeta)$, $V_b(\zeta)$, $\Psi_b(\zeta)$, $W_b(\zeta)$, $U_c(\zeta)$, $\Phi_c(\zeta)$, $V_c(\zeta)$, $\Psi_c(\zeta)$ and $W_c(\zeta)$, have been introduced. In order to simplify the solution process, the resultant force and moment in the shell equivalent to the externally applied torsion as shown in Eq. (8) at the joint end are also expanded as the Fourier series along the pipe wall in the following forms:

$$\tilde{Q}_{b\zeta\zeta}(\zeta, \zeta) = \sum_n \tilde{Q}_{b\zeta\zeta 0}(\zeta) \sin\left(\frac{n\zeta_a}{R_a}\right), \quad \tilde{M}_{b\zeta\zeta}(\zeta, \zeta) = \sum_n \tilde{M}_{b\zeta\zeta 0}(\zeta) \sin\left(\frac{n\zeta_a}{R_a}\right) \quad (13)$$

After substitution of the above relevant solutions into the governing equations in the uniform coordinate system, the coefficients of sine and cosine are collected to obtain a new set of 15 ordinary differential equations involving the above 15 new variables. Here, the detailed new ordinary differential equations for the coupled pipe part are obtained in the following forms:

$$\begin{aligned} A_{p11} \frac{\partial^2 U_{p0}}{\partial \zeta^2} + B_{p11} \frac{\partial^2 \Phi_p}{\partial \zeta^2} + \frac{1}{R_p} A_{p12} \frac{\partial W_p}{\partial \zeta} + (A_{p12} + A_{p661}) \frac{n}{R_p} \frac{\partial V_{p0}}{\partial \zeta} + (B_{p12} + B_{p661}) \frac{n}{R_p} \frac{\partial \Psi_p}{\partial \zeta} - A_{p662} \left(\frac{n}{R_p}\right)^2 U_p \\ - B_{p662} \left(\frac{n}{R_p}\right)^2 \Phi_p = \frac{R_{p0}}{R_p} \left[G_a \left(\frac{U_p - U_c}{h_a} + \frac{h_p \Phi_p + h_c \Phi_c}{2h_a} \right) - \frac{G_a}{2} \left(\frac{\partial W_c}{\partial \zeta} + \frac{\partial W_p}{\partial \zeta} \right) \right] \end{aligned} \quad (14a)$$

$$\begin{aligned} -(A_{p21} + A_{p662}) \frac{n}{R_p} \frac{\partial U_p}{\partial \zeta} - (B_{p21} + B_{p662}) \frac{n}{R_p} \frac{\partial \Phi_p}{\partial \zeta} - \frac{1}{R_p} (A_{p22} + A_{p44}) \frac{n}{R_p} W_p - A_{p22} \left(\frac{n}{R_p}\right)^2 V_p \\ - B_{p22} \left(\frac{n}{R_p}\right)^2 \Psi_p + \frac{1}{R_p} \left(-\frac{1}{R_p} A_{p44} V_p + A_{p44} \Psi_p \right) + A_{p661} \frac{\partial^2 V_p}{\partial \zeta^2} + B_{p661} \frac{\partial^2 \Psi_p}{\partial \zeta^2} \\ = \frac{R_{p0}}{R_p} \left[G_a \left(\frac{V_p - V_c}{h_a} + \frac{h_p \Psi_p + h_c \Psi_c}{2h_a} \right) + \frac{G_a}{2} \left(\frac{n}{R_p} W_p + \frac{n}{R_c} W_c \right) + \frac{G_a}{2} \left(\frac{V_p + V_c}{R_a} + \frac{h_p \Psi_p - h_c \Psi_c}{2R_a} \right) \right] \end{aligned} \quad (14b)$$

$$\begin{aligned} \left(A_{p55} - \frac{1}{R_p} B_{p21} \right) \frac{\partial \Phi_p}{\partial \zeta} + A_{p55} \frac{\partial^2 W_p}{\partial \zeta^2} - \left[A_{p44} \left(\frac{n}{R_p}\right)^2 + \frac{1}{R_p^2} A_{p22} \right] W_p - (A_{p44} + A_{p22}) \frac{n}{R_p^2} V_p \\ + \left(A_{p44} \frac{n}{R_p} - B_{p22} \frac{n}{R_p^2} \right) \Psi_p - \frac{1}{R_p} A_{p21} \frac{\partial U_p}{\partial \zeta} = -\frac{R_{p0}}{R_p} \frac{E_a}{(1+v_a)(1-2v_a)} \left\{ (1-v_a) \frac{W_c - W_p}{h_a} + \frac{v_a}{2} \right. \\ \left. \times \left(\frac{\partial U_{p0}}{\partial \zeta} + \frac{h_p}{2} \frac{\partial \Phi_p}{\partial \zeta} + \frac{\partial U_{c0}}{\partial \zeta} - \frac{h_c}{2} \frac{\partial \Phi_c}{\partial \zeta} \right) + \frac{v_a}{2} \left[\frac{W_p}{R_{p0}} + \frac{R_p}{R_{p0}} \left(\frac{n}{R_p} V_p + \frac{h_p}{2} \frac{n}{R_p} \Psi_p \right) + \frac{W_c}{R_{ci}} + \frac{R_c}{R_{ci}} \left(\frac{n}{R_c} V_c - \frac{h_c}{2} \frac{n}{R_c} \Psi_c \right) \right] \right\} \end{aligned} \quad (14c)$$

$$\begin{aligned} B_{p11} \frac{\partial^2 U_p}{\partial \zeta^2} + D_{p11} \frac{\partial^2 \Phi_p}{\partial \zeta^2} + \left(\frac{1}{R_p} B_{p12} - A_{p55} \right) \frac{\partial W_p}{\partial \zeta} + (B_{p12} + B_{p661}) \frac{n}{R_p} \frac{\partial V_p}{\partial \zeta} + (D_{p12} + D_{p661}) \frac{n}{R_p} \frac{\partial \Psi_p}{\partial \zeta} \\ - \left[A_{p55} + D_{p662} \left(\frac{n}{R_p}\right)^2 \right] \Phi_p - B_{p662} \left(\frac{n}{R_p}\right)^2 U_p \\ = \frac{h_p}{2} \frac{R_{p0}}{R_p} \left[G_a \left(\frac{U_p - U_c}{h_a} + \frac{h_p \Phi_p + h_c \Phi_c}{2h_a} \right) - \frac{G_a}{2} \left(\frac{\partial W_c}{\partial \zeta} + \frac{\partial W_p}{\partial \zeta} \right) \right] \end{aligned} \quad (14d)$$

$$\begin{aligned}
& - (B_{p21} + B_{p661}) \frac{n}{R_p} \frac{\partial U_p}{\partial \zeta} - (D_{p21} + D_{p661}) \frac{n}{R_p} \frac{\partial \Phi_p}{\partial \zeta} - \left(\frac{1}{R_p} B_{p22} - A_{p44} \right) \frac{n}{R_p} W_p - \left[B_{p22} \left(\frac{n}{R_p} \right)^2 - \frac{1}{R_p} A_{p44} \right] V_p \\
& - \left[D_{p22} \left(\frac{n}{R_a} \right)^2 + A_{p44} \right] \Psi_p + \left(B_{p661} + \frac{1}{R_p} D_{p661} \right) \frac{\partial^2 V_p}{\partial \zeta^2} + \left(D_{p661} + \frac{1}{R_p} E_{p661} \right) \frac{\partial^2 \Psi_p}{\partial \zeta^2} \\
& = \frac{h_p}{2} \frac{R_{po}}{R_p} \left[G_a \left(\frac{V_p - V_c}{h_a} + \frac{h_p \Psi_p + h_c \Psi_c}{2h_a} \right) + \frac{G_a}{2} \left(\frac{n}{R_p} W_p + \frac{n}{R_c} W_c \right) + \frac{G_a}{2} \left(\frac{V_p + V_c}{R_a} + \frac{h_p \Psi_p - h_c \Psi_c}{2R_a} \right) \right]
\end{aligned} \quad (14e)$$

In the same manner, the other 10 new ordinary differential equations for the connection coupler part and bare pipe part can be obtained. In order to solve these total 15-ordinary differential equations, the state-space method can be employed to simplify these equations and further obtain a new set of first-order state equations by introducing the following variables:

$$\begin{aligned}
Z_1 &= U_p, \quad Z_2 = Z'_1 = \frac{\partial U_p}{\partial \zeta}, \quad Z_3 = \Phi_p, \quad Z_4 = Z'_3 = \frac{\partial \Phi_p}{\partial \zeta}, \quad Z_5 = V_p, \quad Z_6 = Z'_5 = \frac{\partial V_p}{\partial \zeta}, \\
Z_7 &= \Psi_p, \quad Z_8 = Z'_7 = \frac{\partial \Psi_p}{\partial \zeta}, \quad Z_9 = W_p, \quad Z_{10} = Z'_9 = \frac{\partial W_p}{\partial \zeta}, \quad Z_{11} = U_c, \quad Z_{12} = Z'_{11} = \frac{\partial U_c}{\partial \zeta}, \\
Z_{13} &= \Phi_c, \quad Z_{14} = Z'_{13} = \frac{\partial \Phi_c}{\partial \zeta}, \quad Z_{15} = V_c, \quad Z_{16} = Z'_{15} = \frac{\partial V_c}{\partial \zeta}, \quad Z_{17} = \Psi_c, \quad Z_{18} = Z'_{17} = \frac{\partial \Psi_c}{\partial \zeta}, \\
Z_{19} &= W_c, \quad Z_{20} = Z'_{19} = \frac{\partial W_c}{\partial \zeta} \\
X_1 &= U_b, \quad X_2 = X'_1 = \frac{\partial U_b}{\partial \zeta}, \quad X_3 = \Phi_b, \quad X_4 = X'_3 = \frac{\partial \Phi_b}{\partial \zeta}, \quad X_5 = V_b, \quad X_6 = X'_5 = \frac{\partial V_b}{\partial \zeta}, \\
X_7 &= \Psi_b, \quad X_8 = X'_7 = \frac{\partial \Psi_b}{\partial \zeta}, \quad X_9 = W_b, \quad X_{10} = X'_9 = \frac{\partial W_b}{\partial \zeta}
\end{aligned}$$

Using the above introduced new variables, the relevant differential equations for the connection coupler and coupled pipe in the overlap part can be expressed by a state equation as

$$\{Z\}' = [\mathbf{H}]\{Z\} + [A] \quad (15a)$$

Similarly, a state equation for the bare pipe part can be obtained

$$\{X\}' = [\mathbf{M}]\{X\} \quad (15b)$$

where the non-zero elements of the coefficient matrices $[\mathbf{H}]$ and $[\mathbf{M}]$ are given in details in [Appendix B](#). The 20×1 dimension matrix $[A]$ is related to the actuating piezoelectric layer induced forces and moments due to externally applied electric fields and its non-zero elements can be represented by

$$\begin{aligned}
A(12, 1) &= \frac{D_{c11} \left(N_{c\zeta}^{\text{PZT}} \right)'_{\zeta} - B_{c11} \left(M_{c\zeta}^{\text{PZT}} \right)'_{\zeta}}{A_{c11} D_{c11} - B_{c11}^2}, \quad A(14, 1) = \frac{A_{c11} \left(M_{c\zeta}^{\text{PZT}} \right)'_{\zeta} - B_{c11} \left(N_{c\zeta}^{\text{PZT}} \right)'_{\zeta}}{A_{c11} D_{c11} - B_{c11}^2} \\
A(16, 1) &= \frac{(D_{c661} + E_{c661}/R_c) \left(N_{c\zeta}^{\text{PZT}} \right)'_{\zeta} - B_{c661} \left(M_{c\zeta}^{\text{PZT}} \right)'_{\zeta}}{A_{c661} (D_{c661} + E_{c661}/R_c) - B_{c661} (B_{c661} + D_{c661}/R_c)} \\
A(18, 1) &= \frac{A_{c661} \left(M_{c\zeta}^{\text{PZT}} \right)'_{\zeta} - (B_{c661} + D_{c661}/R_c) \left(N_{c\zeta}^{\text{PZT}} \right)'_{\zeta}}{A_{c661} (D_{c661} + E_{c661}/R_c) - B_{c661} (B_{c661} + D_{c661}/R_c)}, \quad A(20, 1) = -\frac{N_{c\zeta}^{\text{PZT}}}{A_{c55} R_c}
\end{aligned}$$

with the following derivative definitions: $(\cdot)'_x = \frac{\partial(\cdot)}{\partial x}$, $\frac{\partial H(x-x_0)}{\partial x} = \delta(x-x_0)$ and $\frac{\partial^2 H(x-x_0)}{\partial x^2} = \delta'(x-x_0)$.

At the same time, the shear and peel stresses in the adhesive layer can be re-written by the introduced state variables in the following forms:

$$\tau_\zeta = \left[\frac{G_a}{h_a}, 0, \frac{h_p G_a}{2h_a}, 0, 0, 0, 0, 0, -\frac{G_a}{2}, -\frac{G_a}{h_a}, 0, \frac{h_c G_a}{2h_a}, 0, 0, 0, 0, 0, -\frac{G_a}{2} \right] \{Z\} \quad (16a)$$

$$\tau_\zeta = \left[0, 0, 0, 0, \frac{G_a}{h_a} + \frac{G_a}{2R_a}, 0, \frac{h_p G_a}{2h_a} + \frac{h_p G_a}{4R_a}, 0, \frac{G_a}{2} \frac{n}{R_p}, 0, 0, 0, 0, 0, -\frac{G_a}{h_a} + \frac{G_a}{2R_a}, 0, \frac{h_c G_a}{2h_a} - \frac{h_c G_a}{4R_a}, 0, \frac{G_a}{2} \frac{n}{R_c}, 0 \right] \{Z\} \quad (16b)$$

$$p = \frac{E_a}{(1+v_a)(1-2v_a)} \left[0, \frac{v_a}{2}, 0, \frac{v_a}{2} \frac{h_p}{2}, \frac{v_a}{2} \frac{n}{R_{po}}, 0, \frac{v_a}{2} \frac{n}{R_{po}} \frac{h_p}{2}, 0, -\frac{1-v_a}{h_a} + \frac{v_a}{2R_{po}}, 0, 0, \frac{v_a}{2}, 0, -\frac{v_a}{2} \frac{h_c}{2}, \frac{v_a}{2} \frac{n}{R_{ci}}, 0, -\frac{v_a}{2} \frac{n}{R_{ci}} \frac{h_c}{2}, 0, \frac{1-v_a}{h_a} + \frac{v_a}{2R_{ci}}, 0 \right] \{Z\} \quad (16c)$$

Now integrating both sides of Eq. (15a) over dummy variable ϑ from ζ_0 to ζ , the final solution are derived in the following form:

$$Z(\zeta) = e^{\zeta[H]} \{k_1\} + e^{\zeta[H]} \int_{\zeta_0}^{\zeta} e^{-\vartheta[H]} [A] d\vartheta \quad (17a)$$

and the general solution for Eq. (15b) is:

$$X(\zeta) = e^{\zeta[M]} \{k_2\} \quad (17b)$$

where $\{k_1\}$ is a vector with 20 unknown coefficients determined by the relevant boundary and continuity conditions at $\zeta = 0$, l_1 , and $\{k_2\}$ is a vector with 10 unknown coefficients calculated by the boundary and continuity conditions at $\zeta = 0$, l_2 , as shown in Eq. (9). With the help of the first-order shear deformation theory-based strain–stress and strain–displacement relationships, the unknown coefficients $\{k_i\}$ ($i=1, 2$) are determined by the boundary and continuity conditions via the programmed Mathematica software. The peel and shear stresses distribution in the adhesive layer of the composite pipe joint system can be analytically calculated by Eq. (16).

4. Numerical example and discussion

In this section, some detailed numerical analyses were conducted to confirm the integrity of the smart composite pipe joint system subjected to a torsion loading at the joint end. The 54-degree filament-wound E-glass/Derakane 470 composite pipe has been taken as the calculation samples for the composite pipe and connection coupler. In order to improve the electro-mechanical coupling performance of the piezoelectric reinforced composite, we can employ the piezoelectric polymer (PVDF) as the matrix to construct the piezoelectric reinforced composite. The material properties and geometric parameters of the composite pipe and coupler, adhesive and piezoelectric materials used in the detailed simulations are listed below:

Composite layer: $E_1 = 25.2$ GPa, $E_2 = 7.5$ GPa, $G_{12} = 2.4$ GPa, $v_{12} = 0.32$.

Epoxy adhesive: $E_a = 0.96$ GPa, $G_a = 0.34$ GPa, $\mu_3 = 0.412$.

Piezoelectric and polyvinylidene fluoride (PVDF) matrix properties:

Piezoelectric materials (PZT-5H):

$$E_{11} = 127 \text{ GPa}, E_{12} = 80.2 \text{ GPa}, E_{13} = 84.6 \text{ GPa}, E_{33} = 117 \text{ GPa}, E_{44} = 23.0 \text{ GPa}, \\ E_{66} = 23.5 \text{ GPa}, d_{31} = -274 \text{ pC/N}, d_{31} = 593 \text{ pC/N}, d_{31} = 741 \text{ pC/N}, \kappa_{11} = 3130\kappa_0, \\ \kappa_{33} = 3400\kappa_0, \kappa_0 = 8.854 \times 10^{-12} \text{ F/m}.$$

PVDF material properties:

$$E_{11} = E_{22} = 2.0 \text{ GPa}, v = 0.29, G_{12} = 0.775 \text{ GPa}, \\ d_{31} = 22 \text{ pC/N}, \kappa = 13\kappa_0.$$

Geometric parameters: $l_1 = 25.4$ mm; $l_2 = 50.8$ mm; $h_a = 0.0254$ mm. $h_p = h_c = 2.54$ mm, $R_{pi} = 50.8$ mm.

Firstly, based on the developed micromechanical Mori–Tanaka model as given in Appendix A, the effective electro-elastic properties of piezoelectric particles/fiber reinforced composite materials can be theoretically predicted as the functions of volume fraction and aspect ratio ρ of the piezoelectric inclusions, as shown in

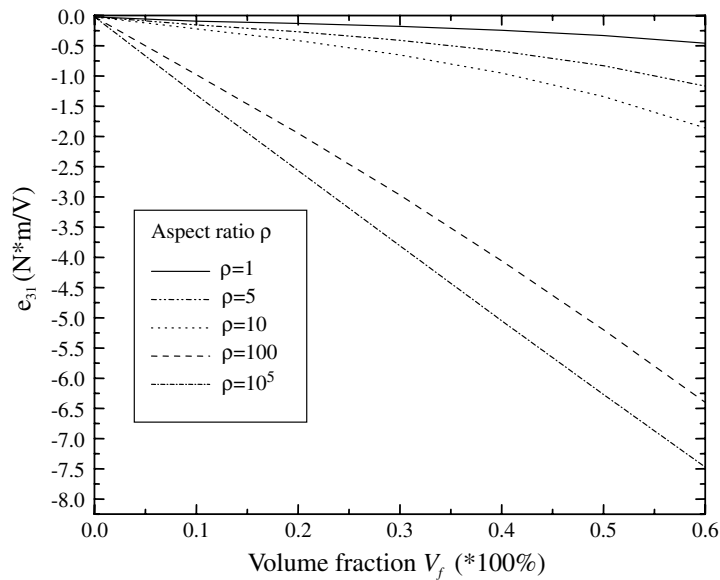


Fig. 6. The effects of the aspect ratio ρ and volume fraction V_f of the reinforcing piezoelectric particle/fiber on the effective piezoelectric constant e_{31} .

Fig. 6. From the calculations in Fig. 6, it is clearly seen that piezoelectric constant e_{31} decreases with the increase of the volume fraction V_f and aspect ratio ρ (Mura, 1982). Here for the convenience of simulation, we can take the piezoelectric reinforced composite materials with a lower fiber aspect ratio (i.e. aspect ratio $\rho = 100$) as the simulation examples.

Furthermore, in order to validate the developed theoretical model, finite element analyses were carried out by using the 3D SOLID45 element in the commercial software (ANSYS) and the results were compared to the theoretical prediction when the developed model was reduced to a conventional composite pipe joint (without the piezoelectric reinforced composite layer) and was subjected to a torsion load of 113 N m at the joint end. The detailed numerical comparison between the present theoretical analyses and the FEM results is depicted in Fig. 7 for the shear and peel stresses at the bond-line. Obviously, the numerical comparison in Fig. 7 verified the integrity of the developed theoretical model for analyzing the adhesively bonded composite pipe joint system subjected to torsion loading.

After the numerical validation of the developed theoretical model and solution method, a smart connection coupler consisting of six layers with the following stacking sequence [Comp/PIEZO1/Comp/Comp/PIEZO2/Comp] and relevant lamina thickness $[\frac{h_c}{6} / \frac{h_c}{6} / \frac{h_c}{6} / \frac{h_c}{6} / \frac{h_c}{6} / \frac{h_c}{6}]$ was considered and defined as Structure #1, as shown in Fig. 8a. The two integrated piezoelectric composite layers PIEZO1 and PIEZO2 are subjected to electric fields E_3^1 and E_3^2 , respectively. Using the above developed theoretical model and solution method, the numerical results for the shear and peel stresses were calculated. Fig. 9 shows the shear and peel stresses distribution along the axial direction at $\xi = 0$ (the adhesive layer bond-line) when the composite pipe joint is subjected to the torsion loading of 113 N m at the joint end and the electric fields of $E_3^1 = E_3^2$ applied to the respective smart piezoelectric composite layers in the smart connection coupler. It is clear that the external electric fields applied to the piezoelectric layer have a significant effect on the peel and shear stresses distribution as shown in Fig. 9, and, the maximum shear and peel stresses always occur at the edges of the coupler end. In order to explicitly figure out the detailed effects of the external electric fields on the shear and peel stresses in the adhesive layer bond-line, the maximum shear and peel stresses in the adhesive layer for the following four cases of applied electric fields were studied and discussed: Case 1, $E_3^2 = E_3^1$; Case 2, $E_3^2 = -E_3^1$; Case 3, $E_3^1 \neq 0$, $E_3^2 = 0$; and Case 4, $E_3^1 = 0$, $E_3^2 \neq 0$. Using the definitions of the resultant force and moment equations in Eq. (4) and the stacking sequence, we calculated the relevant forces and moments in the integrated piezoelectric layers caused by the applied electric fields in the above study cases for further calculations in Eqs. (15)–(17). Here, Fig. 10 numerically presents the applied electric fields v.s. the maximum shear and peel stresses

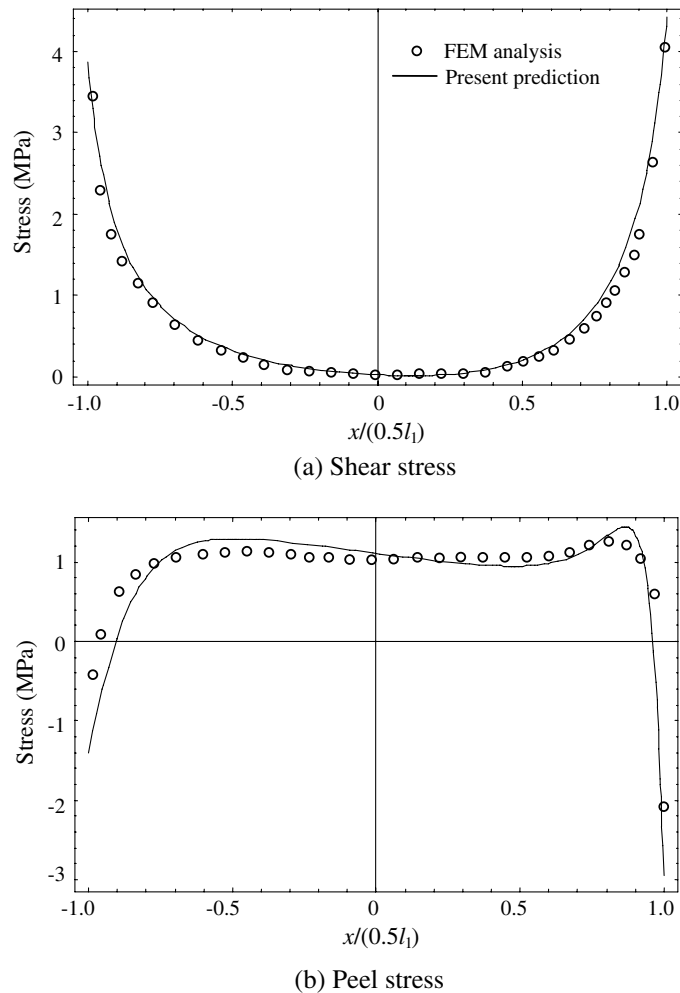


Fig. 7. The detailed numerical comparison between the FEM analysis and theoretical prediction of the shear stress τ_c (a) and peel stress (b) distribution in the adhesive layer of a conventional pipe joint.

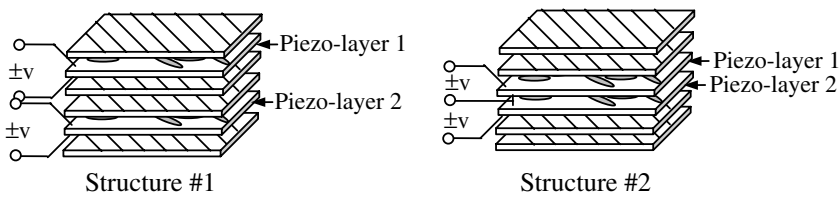


Fig. 8. The schematic shows of studied cases of the smart laminated connection coupler structural characteristics.

in the adhesive layer. It is seen that the maximum shear and peel stresses can be adaptively controlled by adjusting the amplitude and polarity of the electric fields applied to the integrated piezoelectric composite layers. This means that the joint system strength improvement can be realized by choosing reasonable electric fields applied to the smart coupler. Indeed, the different electric fields can result in different strength improvement effects. For the present four study cases, it is found that the applied electric field in Case 3 has less effect on both the shear and peel stresses in the adhesive layer with comparison to the other study cases. However, the applied electric field in Case 4, which is similar to that in Case 3, is more effective in controlling the shear and peel stresses, which is similar to the effectiveness of the Case 1 as indicated in Fig. 10. Compared to the

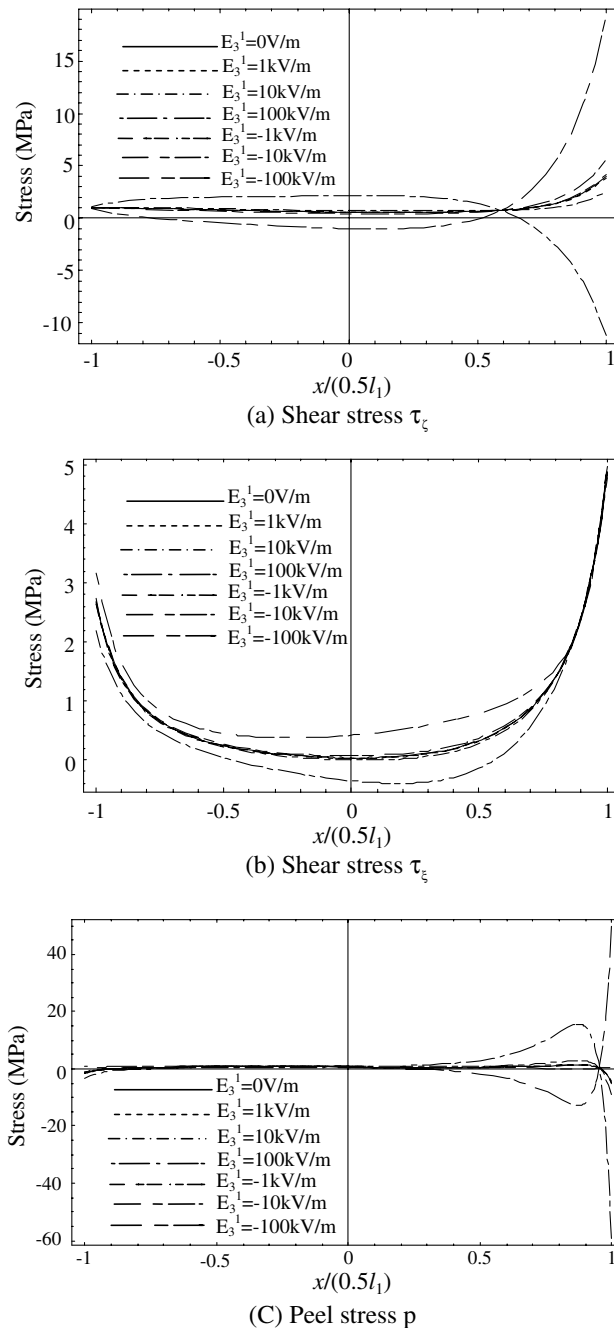


Fig. 9. The influence of the applied electric fields in Case 1 on the shear and peel stresses distribution in the adhesive layer for the Structure #1 coupler.

Case 2, the applied electric field of Case 1 always motivates opposite action in controlling the maximum shear and peel stresses. It is also indicated that the integrated piezoelectric layer has a small influence on the shear stress τ_{ξ} ; however, it has a significant effect on adjusting the shear stress τ_{ζ} and peel stress p as shown in Fig. 10. It is noted from Fig. 10b that a jump of the maximum shear stress τ_{ξ} occurs when the applied electric field reaches a certain value. This is because the maximum shear stress τ_{ξ} will be shifted from the right end-edge ($x_1 = l_1$) to the left end-edge ($x_1 = 0$) when the applied electric field is high enough to change the stress distribution in the adhesive bond-line. From the results in Fig. 10, it is also seen that the shear stress τ_{ζ} and

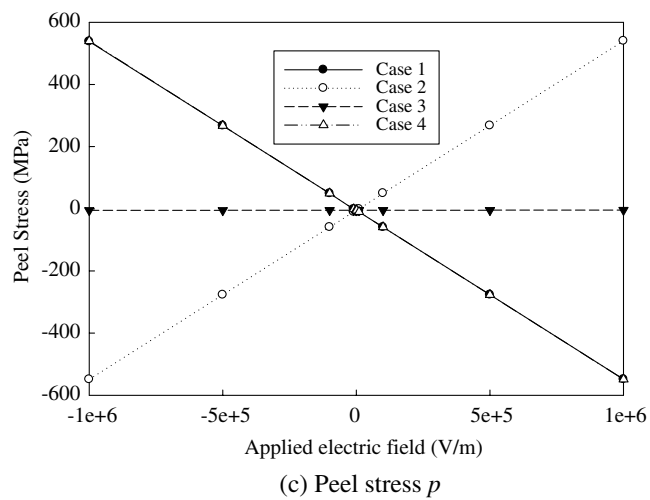
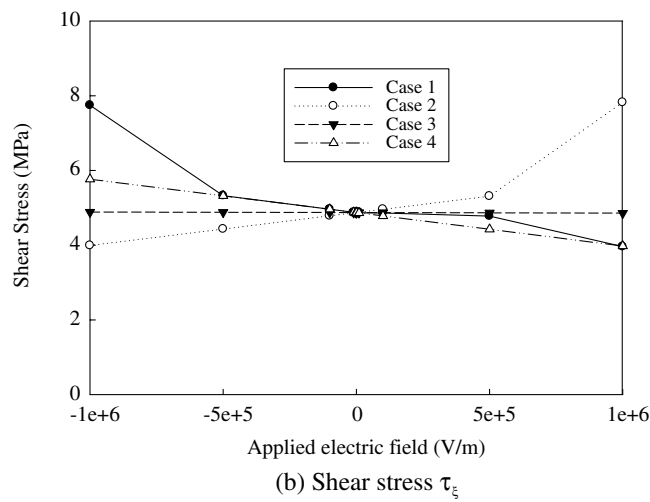
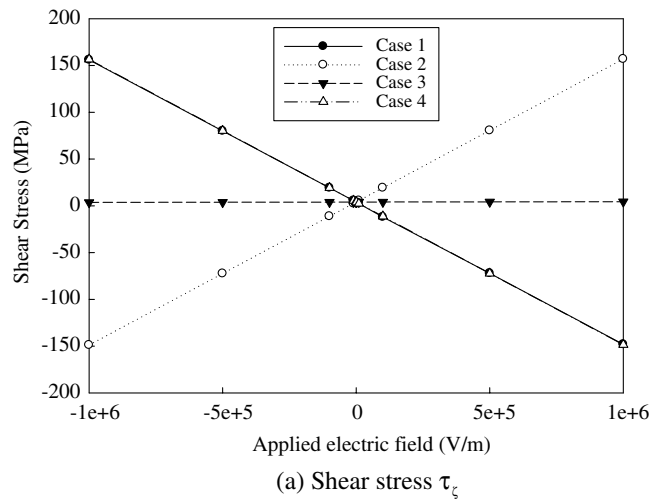


Fig. 10. The influence of the applied electric field in various cases on the maximum shear and peel stresses in the adhesive layer of the smart composite pipe joint with the Structure #1 coupler.

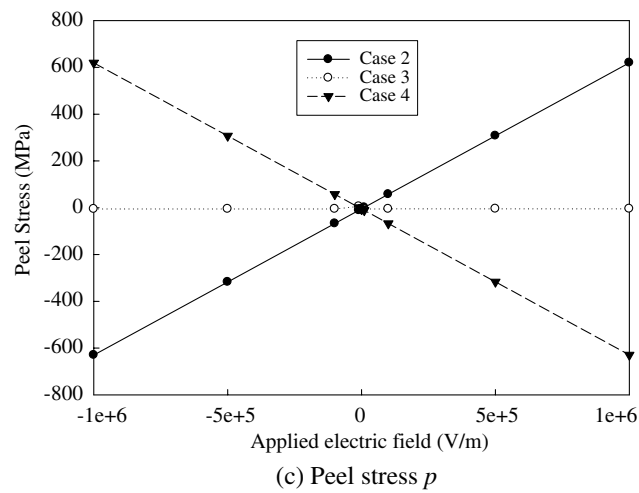
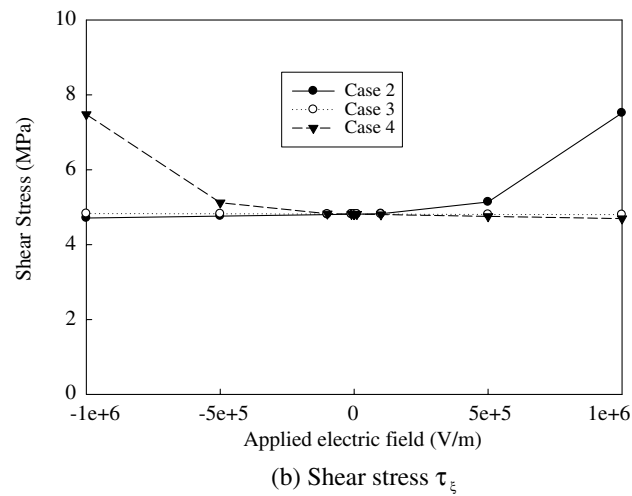
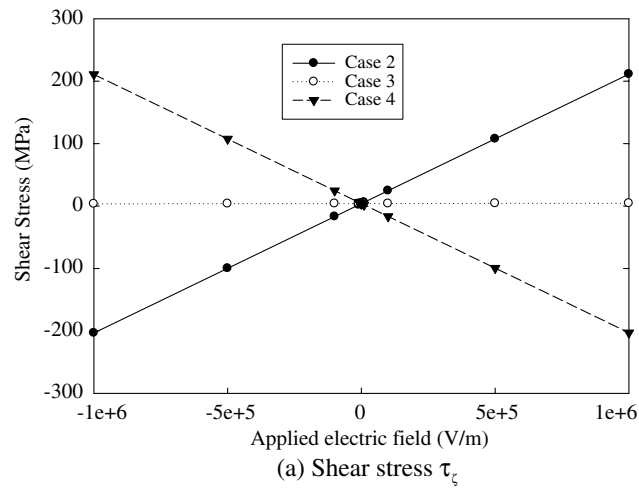


Fig. 11. The influence of the applied electric field in various cases on the maximum shear and peel stresses in the adhesive layer of the smart composite pipe joint with the Structure #2 coupler.

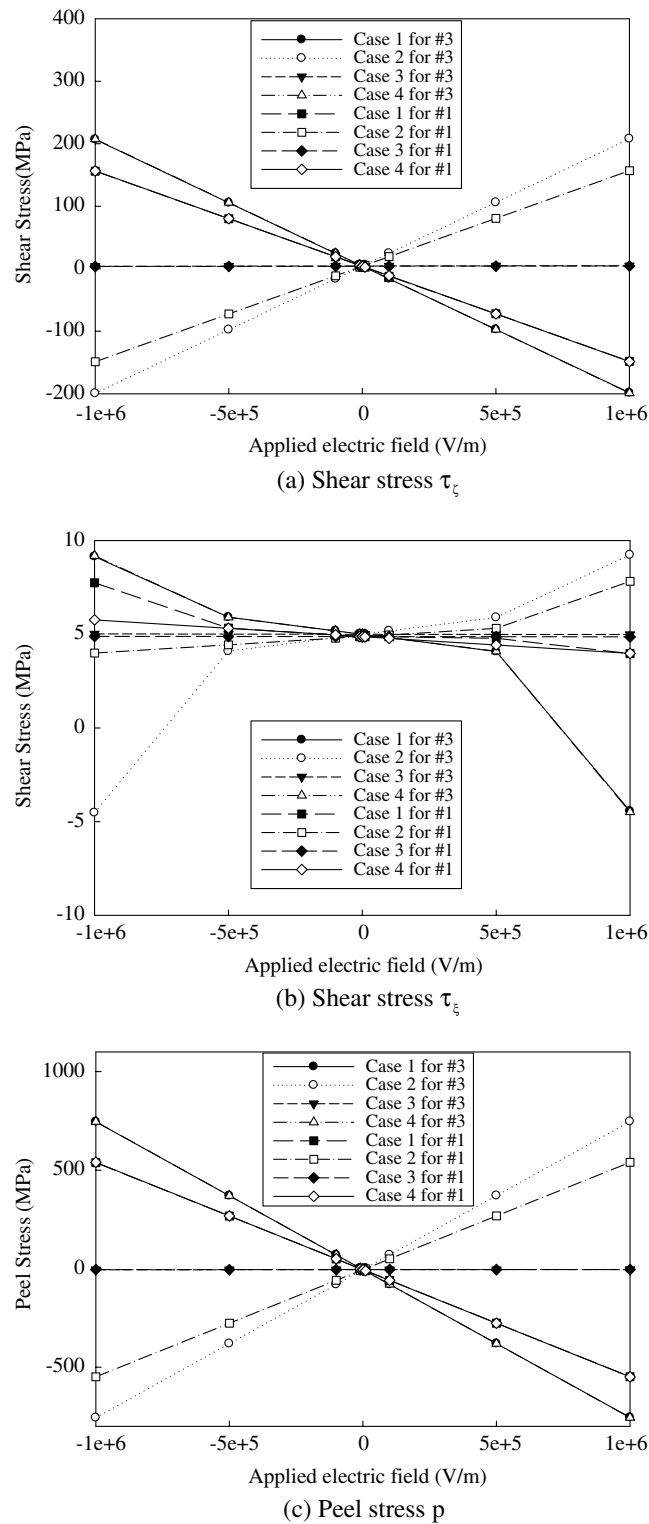


Fig. 12. Numerical comparison of the detailed influence of the applied electric field in various cases on the maximum shear and peel stresses in the adhesive layer for the smart composite pipe joint with the Structure #1 and #3 coupler, respectively.

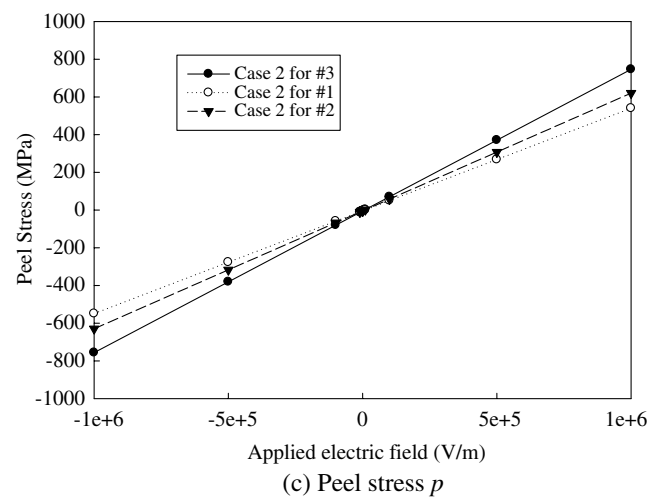
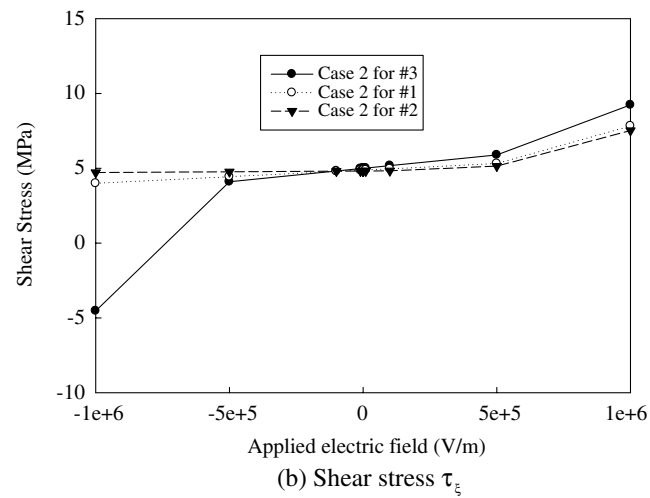
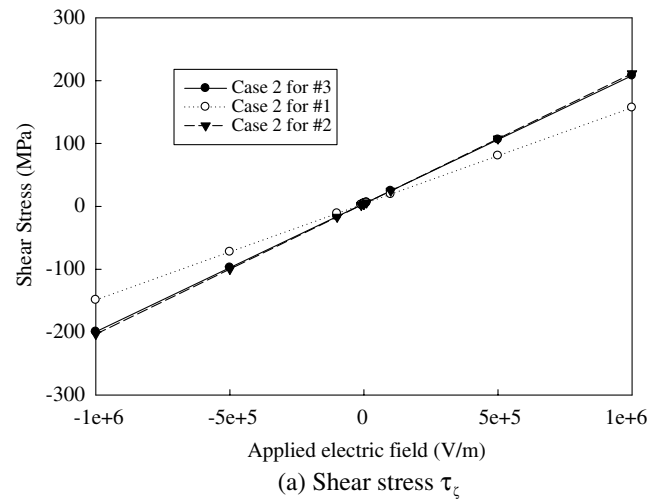


Fig. 13. Numerical comparison of the maximum shear and peel stresses in the adhesive layer of the smart composite pipe joints with various coupler structures in Case 2 loading.

peel stress p at the edge of the joint end can be reduced to zero by selecting suitable applied electric fields in the integrated piezoelectric composite layers.

Further in order to interpret the effect of the stacking sequence of the integrated piezoelectric layers on the smart coupler, a new stacking sequence for the six layers smart connection coupler was set as [Comp/Comp/PIEZO1/PIEZO2/Comp/Comp] with the relevant lamina thickness $[\frac{h_c}{6}/\frac{h_c}{6}/\frac{h_c}{6}/\frac{h_c}{6}/\frac{h_c}{6}/\frac{h_c}{6}]$, named as Structure #2 (see Fig. 8b). Fig. 11 depicts the detailed effects of the applied electric fields in Case 2, Case 3 and Case 4, as defined above, on the maximum shear and peel stresses in the adhesive layer. It is seen that the applied electric field can also achieve a stress controlling function similar to the above studied Structure #1. It is also seen that the applied electric fields in Case 3 always have less effect on the maximum shear and peel stresses than the other study cases. Furthermore, a case by case comparison to the results in Fig. 10, it is seen that the present stacking sequence (i.e. Structure #2) can achieve a more efficient stress controlling function in the shear stress τ_ζ and peel stress p ; for the shear stress τ_ξ , however, this higher efficiency only occurs in some special electric field zones, as shown in Fig. 11b.

Furthermore, a third type of smart composite coupler (i.e. Structure #3) was taken into consideration for studying the effect of the integrated piezoelectric layer thickness on the overall shear and peel stress distributions. Structure #3 has the same stacking sequence [Comp/PIEZO1/Comp/Comp/PIEZO2/Comp] as Structure #1, but with different lamina thicknesses $[\frac{h_c}{8}/\frac{h_c}{4}/\frac{h_c}{8}/\frac{h_c}{8}/\frac{h_c}{4}/\frac{h_c}{8}]$. Fig. 12 presents the effects of the applied electric field on the maximum shear and peel stresses in the adhesive layer, along with the results for Structure #1. With comparison to the numerical results for Structure #1, the results for Structure #3 numerically confirm that the stress controlling effect in Structure #3 is similar to that in Structure #1. However, more improvement is found for Structure #3, i.e., increasing the thickness of the piezoelectric composite layers in the connection coupler.

Finally, the controlling efficiency of the integrated piezoelectric reinforced composite layers in the various coupler structures is studied in detail. From the above numerical simulations, it is clearly found that the study Case 2 can accomplish better stress controlling function in the adhesive layer and thus can be taken as a comparison example. Fig. 13 illustrates the maximum shear and peel stresses controlling efficiency of the three coupler Structures when the integrated piezoelectric layers are subjected to the electric field loading in Case 2. From Fig. 13, it is explicitly shown that the Structure #3 can achieve better stress controlling efficiency than the others.

5. Conclusion

In order to adaptively improve the pipe joint strength and overcome the limitation of brittle piezoelectric ceramics in practical applications, a smart composite pipe joint system was developed by using the flexible piezoelectric reinforced polymer composite. For better understanding and optimally designing the developed smart composite pipe joint system subjected to a torsion load, the following outlines were conducted and achieved:

- (1) A first-order shear deformation theory-based theoretical model was developed for the basis behavior analyses of the developed smart pipe joint system.
- (2) With the help of the Levy solution and the state-space method, the detailed shear and peel stresses distribution in the adhesive layer were analytically predicted and analyzed. The electro-elastic properties of the piezoelectric particle/fiber reinforced polymer composite were determined using the Mori–Tanaka's method.
- (3) The effect of the stacking sequence and thickness of the integrated piezoelectric composite layers as well as the applied electric fields on reducing the stress concentration in the adhesive layer were evaluated by simulating three types of coupler structure.
- (4) From the present theoretical studies, it is found that the stress concentration in the adhesive layer bond-line can be significantly reduced by adjusting the stacking sequence of the coupler, the piezoelectric layer thickness, and the applied electric fields.
- (5) Among the four cases considered here, Case 2 is the most effective in controlling the stress concentration. For the three coupler structures studied, Structure #3 is the most effective.

Acknowledgement

This project is based upon the work supported by the Louisiana Space Consortium under Contract Number NASA/LEQSF(2006)-DART-26. This study is also partially sponsored by NASA/EPSCoR under Contract Number NASA/LEQSF(2007-10)-Phase3-01. The support is greatly appreciated.

Appendix A. Electro-elastic properties of piezoelectric particle/fiber/wire reinforced composite

Because of the high electro-mechanical coupling and flexible performance of the piezoelectric particle/fiber/wire reinforced polymer composites, they have been successfully applied in the engineering field as transducers/actuators, including underwater sonar and biomedical imaging applications. In order to analyze the electro-elastic properties of the piezoelectric reinforced composite, here we developed a micromechanics method to predict the effective piezoelectric coupling properties on the basis of Mori–Tanaka's method.

Considering a piezoelectric reinforced composites consisting of a matrix with the electro-elastic moduli E_m and the reinforced ellipsoidal piezoelectric particles with electro-elastic moduli E_{in} as defined in the previous works (Cheng et al., 1999, 2000, 2002), we can use the equivalent inclusion method and Mori–Tanaka's average field theory to obtain the stress and electric displacement in the representative particle and the matrix when the composite is subjected to the far-field applied stress and electric displacement Σ^0 in the following formation:

In the matrix, we should consider the disturbance field Σ^1 caused by the presence of the reinforcing piezoelectric particles (inclusions) and have:

$$\Sigma_m = \Sigma^0 + \Sigma^1 = E_m(Z^0 + Z^1) \quad (A.1)$$

In the inclusion, we must take the perturbation and interaction of the reinforcing piezoelectric particles into consideration as Σ^{pt} and yield:

$$\Sigma_{in} = \Sigma^0 + \Sigma^1 + \Sigma^{pt} = E_{in}(Z^0 + Z^1 + Z^{pt}) = E_m(Z^0 + Z^1 + Z^{pt} - Z^*) \quad (A.2)$$

where Z^* is the fictitious eigenfield due to the inhomogeneity of the reinforcing particles. And, the perturbed field Z^{pt} can be obtained in terms of the electro-elastic Eshelby's tensor S as shown in the previous works of (Wang, 1992; Cheng et al., 1999, 2000, 2002) as

$$Z^{pt} = SZ^* \quad (A.3)$$

Further, when the composite is subjected to a far-field traction and electric displacement, $\Sigma_{ij}^0 n_i$, on the boundary with outward unit normal vector n_i , the average field of the piezoelectric reinforced composite can be obtained by the Mori–Tanaka's mean field approach as

$$\langle \Sigma \rangle = \frac{1}{V} \int_{\Omega_m} \Sigma_m dv + \frac{1}{V} \int_{\Omega_{in}} \Sigma_{in} dv \quad (A.4)$$

After substituting the fields inside the matrix and inclusions as shown in Eqs. (A.1) and (A.2) into the above equation, the disturbed field Z^1 can be obtained with Eq. (A.3) as

$$Z^1 = -V_f(S - I)Z^* \quad (A.5)$$

where V_f is the volume fraction of the reinforcing piezoelectric particles. I is a 9×9 dimension identity matrix.

Then, using Eq. (A.5), we can find the fictitious eigenfield Z^* due to the inhomogeneity from Eq. (A.2) as

$$Z^* = [V_f(E_{in} - E_m)(S - I) - E_{in}S + E_m(S - I)]^{-1}(E_{in} - E_m)Z^0 \quad (A.6)$$

Therefore, the overall strain and electric field denoted by $\langle Z \rangle$ can be obtained as the weighted average of each phase of piezoelectric reinforced composite as follows:

$$\langle Z \rangle = \frac{1}{V} \int_{\Omega_m} Z_m dv + \frac{1}{V} \int_{\Omega_{in}} Z_{in} dv = \frac{1}{V} \int_{\Omega_m} (Z^0 + Z^1) dv + \frac{1}{V} \int_{\Omega_{in}} (Z^0 + Z^1 + Z^{pt}) dv = Z^0 + V_f Z^* \quad (A.7)$$

Now, considering the application of the overall far-field to the piezoelectric composite, we have the general electro-elastic constitutive relationship as follows:

$$\langle \Sigma \rangle = E^* \langle Z \rangle = \Sigma^0 \quad (\text{A.8})$$

Further combining the above Eqs. (A.6)–(A.8), we can obtain the analytical expression for the effective electro-elastic properties of piezoelectric particle reinforced composite as follows:

$$E^* = \{I + V_f[V_f(E_{in} - E_m)(S - I) - E_{in}S + E_m(S - I)]^{-1}(E_{in} - E_m)\}^{-1}E_m \quad (\text{A.9})$$

Appendix B. The element of matrix [H] and [M]

Based on the introduced new state variables, the resultant governing equations for the overlapping pipe and the connection coupler, as shown in Eq. (14a)–(14e), are presented in the matrix form as

$$[\Xi]\{Z\}' = [A]\{Z\} \quad (\text{B.1})$$

further, the matrix [H] in Eq. (15a) is obtained as

$$[H] = [\Xi]^{-1}[A] \quad (\text{B.2})$$

where the non-zero elements of the matrix are listed as follows:

$$\begin{aligned} \Xi(i, i) &= 1 \quad (i = 1, 3, 5, \dots, 19) \\ \Xi(2, 2) &= A_{p11}, \quad \Xi(2, 4) = B_{p11}, \quad \Xi(4, 2) = B_{p11}, \quad \Xi(4, 4) = D_{p11}, \quad \Xi(6, 6) = A_{p661}, \\ \Xi(6, 8) &= B_{p661}, \quad \Xi(8, 6) = \left(B_{p661} + \frac{D_{p661}}{R_p}\right), \quad \Xi(8, 8) = \left(D_{p661} + \frac{E_{p661}}{R_p}\right), \quad \Xi(10, 10) = A_{p55}, \\ \Xi(12, 12) &= A_{c11}, \quad \Xi(12, 14) = B_{c11}, \quad \Xi(14, 12) = B_{c11}, \quad \Xi(14, 14) = D_{c11}, \quad \Xi(16, 16) = A_{c661}, \\ \Xi(16, 18) &= B_{c661}, \quad \Xi(18, 16) = \left(B_{c661} + \frac{D_{c661}}{R_c}\right), \quad \Xi(18, 18) = \left(D_{c661} + \frac{E_{c661}}{R_c}\right), \quad \Xi(20, 20) = A_{c55} \end{aligned}$$

and

$$\begin{aligned} A(i, i+1) &= 1, \quad (i = 1, 3, 5, 7 \dots 19) \\ A(2, 1) &= A_{p662} \left(\frac{n}{R_p}\right)^2 + \frac{R_{po}}{R_p} \frac{G_a}{h_a}, \quad A(2, 3) = B_{p662} \left(\frac{n}{R_p}\right)^2 + \frac{R_{po}}{R_p} \frac{G_a h_p}{2h_a}, \quad A(2, 6) = -(A_{p12} + A_{p661}) \frac{n}{R_p}, \\ A(2, 8) &= -(B_{p12} + B_{p661}) \frac{n}{R_p}, \quad A(2, 10) = -\frac{A_{p12}}{R_p} - \frac{R_{po}}{R_p} \frac{G_a}{2}, \quad A(2, 11) = -\frac{R_{po}}{R_p} \frac{G_a}{h_a}, \\ A(2, 13) &= \frac{R_{po}}{R_p} \frac{G_a h_c}{2h_a}, \quad A(2, 20) = -\frac{R_{po}}{R_p} \frac{G_a}{2}, \quad A(4, 1) = B_{p662} \left(\frac{n}{R_p}\right)^2 + \frac{h_p}{2} \frac{R_{po}}{R_p} \frac{G_a}{h_a}, \\ A(4, 3) &= A_{p55} + D_{p662} \left(\frac{n}{R_p}\right)^2 + \frac{h_p}{2} \frac{R_{po}}{R_p} \frac{G_a h_p}{2h_a}, \quad A(4, 6) = -(B_{p12} + B_{p661}) \frac{n}{R_p}, \\ A(4, 8) &= -(D_{p12} + D_{p661}) \frac{n}{R_p}, \quad A(4, 10) = -\left(\frac{B_{p12}}{R_p} - A_{p55}\right) - \frac{h_a}{2} \frac{R_{po}}{R_p} \frac{G_a}{2}, \quad A(4, 11) = -\frac{h_p}{2} \frac{R_{po}}{R_p} \frac{G_a}{h_a}, \\ A(4, 13) &= \frac{h_p}{2} \frac{R_{po}}{R_p} \frac{G_a h_c}{2h_a}, \quad A(4, 20) = -\frac{h_p}{2} \frac{R_{po}}{R_p} \frac{G_a}{2}, \quad A(6, 2) = (A_{p21} + A_{p662}) \frac{n}{R_p}, \\ A(6, 4) &= (B_{p21} + B_{p662}) \frac{n}{R_p}, \quad A(6, 5) = A_{p22} \left(\frac{n}{R_p}\right)^2 + \frac{A_{p44}}{R_p^2} + \frac{R_{po}}{R_p} \left(\frac{G_a}{h_a} + \frac{G_a}{2R_a}\right), \end{aligned}$$

$$\begin{aligned}
A(6, 7) &= B_{p22} \left(\frac{n}{R_p} \right)^2 - \frac{A_{p44}}{R_p} + \frac{R_{po}}{R_p} \left(\frac{G_a h_p}{2h_a} + \frac{G_a h_p}{4R_a} \right), \quad A(6, 9) = (A_{p22} + A_{p44}) \frac{n}{R_p^2} + \frac{R_{po}}{R_p} \frac{G_a n}{2R_p}, \\
A(6, 15) &= \frac{R_{po}}{R_p} \left(-\frac{G_a}{h_a} + \frac{G_a}{2R_a} \right), \quad A(6, 17) = \frac{R_{po}}{R_p} \left(\frac{G_a h_c}{2h_a} - \frac{G_a h_c}{4R_a} \right), \quad A(6, 19) = \frac{R_{po}}{R_p} \frac{G_a n}{2R_c}, \\
A(8, 2) &= (B_{p21} + B_{p662}) \frac{n}{R_p}, \quad A(8, 4) = (D_{p21} + D_{p662}) \frac{n}{R_p}, \quad A(8, 5) = B_{p22} \left(\frac{n}{R_p} \right)^2 - \frac{A_{p44}}{R_p} + \frac{2R_{po}}{h_p R_p} \left(\frac{G_a}{h_a} + \frac{G_a}{2R_a} \right), \\
A(8, 7) &= D_{p22} \left(\frac{n}{R_p} \right)^2 + \frac{h_p}{2} \frac{R_{po}}{R_p} \left(\frac{G_a h_p}{2h_a} + \frac{G_a h_p}{4R_a} \right), \quad A(8, 9) = \left(\frac{B_{p22}}{R_p} - A_{p44} \right) \frac{n}{R_p} + \frac{h_p}{2} \frac{R_{po}}{R_p} \frac{G_a n}{2R_p}, \\
A(8, 15) &= \frac{h_p}{2} \frac{R_{po}}{R_p} \left(-\frac{G_a}{h_a} + \frac{G_a}{2R_a} \right), \quad A(8, 17) = \frac{h_p}{2} \frac{R_{po}}{R_p} \left(\frac{G_a h_c}{2h_a} - \frac{G_a h_c}{4R_a} \right), \quad A(8, 19) = \frac{h_p}{2} \frac{R_{po}}{R_p} \frac{G_a n}{2R_c}, \\
A(10, 2) &= \frac{A_{p21}}{R_p} + a \frac{v_a}{2}, \quad A(10, 4) = - \left(A_{p55} - \frac{B_{p21}}{R_p} \right) + a \frac{v_a}{2} \frac{h_p}{2}, \quad A(10, 5) = (A_{p44} + A_{p22}) \frac{n}{R_p^2} + a \frac{v_a}{2} \frac{R_{po}}{R_p} \frac{n}{R_p}, \\
A(10, 7) &= - \left(A_{p44} \frac{n}{R_p} - B_{p22} \frac{n}{R_p^2} \right) + a \frac{v_a}{2} \frac{R_{po}}{R_p} \frac{n}{R_p} \frac{h_p}{2}, \quad A(10, 9) = A_{p44} \frac{n^2}{R_p^2} + \frac{A_{p22}}{R_p^2} - a \frac{(1 - v_a)}{h_a} + a \frac{v_a}{2} \frac{1}{R_{po}}, \\
A(10, 12) &= a \frac{v_a}{2}, \quad A(10, 14) = -a \frac{v_a}{2} \frac{h_c}{2}, \quad A(10, 15) = a \frac{v_a}{2} \frac{R_c}{R_{ci}} \frac{n}{R_c}, \quad A(10, 17) = -a \frac{v_a}{2} \frac{R_c}{R_c} \frac{n}{R_{ci}} \frac{h_c}{2}, \\
A(10, 19) &= a \frac{(1 - v_a)}{h_a} + a \frac{v_a}{2} \frac{1}{R_{ci}}, \quad A(12, 1) = -\frac{R_{ci}}{R_c} \frac{G_a}{h_a}, \quad A(12, 3) = -\frac{R_{ci}}{R_c} \frac{G_a h_p}{2h_a}, \quad A(12, 10) = \frac{R_{ci}}{R_c} \frac{G_a}{2}, \\
A(12, 11) &= A_{c662} \left(\frac{n}{R_c} \right)^2 + \frac{R_{ci}}{R_c} \frac{G_a}{h_a}, \quad A(12, 13) = B_{c662} \left(\frac{n}{R_c} \right)^2 - \frac{R_{ci}}{R_c} \frac{G_a h_c}{2h_a}, \\
A(12, 16) &= -(A_{c12} + A_{c661}) \frac{n}{R_c}, \quad A(12, 18) = -(B_{c12} + B_{c661}) \frac{n}{R_c}, \quad A(12, 20) = -\frac{A_{c12}}{R_c} + \frac{R_{ci}}{R_c} \frac{G_a}{2}, \\
A(14, 1) &= \frac{h_c}{2} \frac{R_{ci}}{R_c} \frac{G_a}{h_a}, \quad A(14, 3) = \frac{h_c}{2} \frac{R_{ci}}{R_c} \frac{G_a h_p}{2h_a}, \quad A(14, 10) = -\frac{h_c}{2} \frac{R_{ci}}{R_c} \frac{G_a}{2}, \\
A(14, 11) &= B_{c662} \left(\frac{n}{R_c} \right)^2 - \frac{h_c}{2} \frac{R_{ci}}{R_c} \frac{G_a}{h_a}, \quad A(14, 13) = A_{c55} + D_{c662} \left(\frac{n}{R_c} \right)^2 + \frac{h_c}{2} \frac{R_{ci}}{R_c} \frac{G_a h_c}{2h_a}, \\
A(14, 16) &= -(B_{c12} + B_{c661}) \frac{n}{R_c}, \quad A(14, 20) = - \left(\frac{B_{c12}}{R_c} - A_{c55} \right) - \frac{h_c}{2} \frac{R_{ci}}{R_c} \frac{G_a}{2}, \\
A(16, 5) &= -\frac{R_{ci}}{R_c} \left(\frac{G_a}{h_a} + \frac{G_a}{2R_a} \right), \quad A(16, 7) = -\frac{R_{ci}}{R_c} \left(\frac{G_a h_p}{2h_a} + \frac{G_a h_p}{4R_a} \right), \quad A(16, 9) = -\frac{R_{ci}}{R_c} \frac{G_a n}{2R_p}, \\
A(16, 12) &= (A_{c21} + A_{c662}) \frac{n}{R_c}, \quad A(16, 14) = (B_{c21} + B_{c662}) \frac{n}{R_c}, \\
A(16, 15) &= A_{c22} \left(\frac{n}{R_c} \right)^2 + \frac{A_{c44}}{R_c^2} + \frac{R_{ci}}{R_c} \left(\frac{G_a}{h_a} - \frac{G_a}{2R_a} \right), \quad A(16, 17) = B_{c22} \left(\frac{n}{R_c} \right)^2 - \frac{A_{c44}}{R_c} - \frac{R_{ci}}{R_c} \left(\frac{G_a h_c}{2h_a} - \frac{G_a h_c}{4R_a} \right), \\
A(16, 19) &= (A_{c22} + A_{c44}) \frac{n}{R_c^2} - \frac{R_{ci}}{R_c} \frac{G_a n}{2R_c}, \quad A(18, 5) = \frac{h_c}{2} \frac{R_{ci}}{R_c} \left(\frac{G_a}{h_a} + \frac{G_a}{2R_a} \right), \\
A(18, 7) &= \frac{h_c}{2} \frac{R_{ci}}{R_c} \left(\frac{G_a h_p}{2h_a} + \frac{G_a h_p}{4R_a} \right), \quad A(18, 9) = \frac{h_c}{2} \frac{R_{ci}}{R_c} \frac{G_a n}{2R_p}, \quad A(18, 12) = (B_{c21} + B_{c662}) \frac{n}{R_c},
\end{aligned}$$

$$\begin{aligned}
A(18, 14) &= (D_{c21} + D_{c662}) \frac{n}{R_c}, \quad A(18, 15) = B_{c22} \left(\frac{n}{R_c} \right)^2 - \frac{A_{c44}}{R_c} + \frac{h_c}{2} \frac{R_{ci}}{R_c} \left(-\frac{G_a}{h_a} + \frac{G_a}{2R_a} \right), \\
A(18, 17) &= D_{c22} \left(\frac{n}{R_c} \right)^2 + A_{c44} + \frac{h_c}{2} \frac{R_{ci}}{R_c} \left(\frac{G_a h_c}{2h_a} - \frac{G_a h_c}{4R_a} \right), \quad A(18, 19) = \left(\frac{B_{c22}}{R_c} - A_{c44} \right) \frac{n}{R_c} + \frac{h_c}{2} \frac{R_{ci}}{R_c} \frac{G_a n}{2R_c}, \\
A(20, 2) &= b \frac{v_a}{2}, \quad A(20, 4) = b \frac{v_a}{2} \frac{h_p}{2}, \quad A(20, 5) = b \frac{v_a}{2} \frac{R_p}{R_{po}} \frac{n}{R_p}, \quad A(20, 7) = b \frac{v_a}{2} \frac{R_p}{R_{po}} \frac{n}{R_p} \frac{h_p}{2}, \\
A(20, 9) &= -b \frac{(1 - v_a)}{h_a} + b \frac{v_a}{2} \frac{1}{R_{po}}, \quad A(20, 12) = \frac{A_{c21}}{R_c} + b \frac{v_a}{2}, \\
A(20, 14) &= - \left(A_{c55} - \frac{B_{c21}}{R_c} \right) - b \frac{v_a}{2} \frac{h_c}{2}, \quad A(20, 15) = (A_{c44} + A_{c22}) \frac{n}{R_c^2} + b \frac{v_a}{2} \frac{R_{ci}}{R_c} \frac{n}{R_c}, \\
A(20, 17) &= - \left(A_{c44} \frac{n}{R_c} - B_{c22} \frac{n}{R_c^2} \right) - b \frac{v_a}{2} \frac{R_{ci}}{R_c} \frac{n}{R_c} \frac{h_c}{2}, \quad A(20, 19) = A_{c44} \frac{n^2}{R_c^2} + \frac{A_{c22}}{R_c^2} + b \frac{(1 - v_a)}{h_a} + b \frac{v_a}{2} \frac{1}{R_{ci}},
\end{aligned}$$

with the following definitions:

$$a = -\frac{R_{po}}{R_p} \frac{E_a}{(1 + v_a)(1 - 2v_a)}, \quad b = \frac{R_{ci}}{R_c} \frac{E_a}{(1 + v_a)(1 - 2v_a)}$$

Similarly, the displacement-based governing equations for the bare pipe part can be obtained by neglecting the right terms of Eqs. (14a)–(14e) and are further presented in the matrix form as follows:

$$[II]\{X\}' = [B]\{X\}, \quad (B.3)$$

where the $[II]$ is a 10×10 dimensional matrix, in which the elements are equal to the relevant elements of the first 10 columns in the first 10 rows of matrix $[E]$. The matrix $[B]$ is also a 10×10 dimensional matrix, which are equal to the part of the first 10 rows \times 10 columns of matrix $[A]$, only by neglecting the underlined terms in the relevant elements. Then, the matrix $[M]$ can be obtained by:

$$[M] = [II]^{-1}[B] \quad (B.4)$$

References

- Adams, R.D., Peppiatt, N.A., 1977. Stress analysis of adhesive bonded tubular lap joint. *Journal of Adhesion* 9, 1–18.
- Adams, R.D., Wake, W.C., 1984. *Structural Adhesive Joints in Engineering*. Elsevier, London.
- Albat, A.M., Romilly, D.P., 1999. A direct linear-elastic analysis of double symmetric bonded joints and reinforcements. *Composites Science and Technology* 59, 1127–1137.
- Chen, D., Cheng, S., 1992a. Torsional stresses in tubular lap joints with tapered adherends. *Journal of Engineering Mechanics-ASCE* 118 (9), 1962–1973.
- Chen, D., Cheng, S., 1992b. Torsional stress in tubular lap joints. *International Journal of Solids and Structures* 29 (7), 845–853.
- Cheng, J.Q., Taheri, F., 2005. A novel smart adhesive joint system. *Smart Materials and Structures* 14 (5), 971–981.
- Cheng, J.Q., Taheri, F., 2006. A smart single-lap adhesive joint integrated with partially distributed piezoelectric patches. *International Journal of Solids and Structures* 43 (5), 1079–1092.
- Cheng, S., Chen, D., Shi, Y.P., 1991. Analysis of adhesive-bonded joints with nonidentical adherends. *Journal of Engineering Mechanics* 117 (3), 605–623.
- Cheng, J.Q., Wang, B., Du, S.Y., 1999. Effective electroelastic properties of polycrystalline ferroelectric ceramics predicted by a statistical model. *Acta Mechanica* 138 (3–4), 163–175.
- Cheng, J.Q., Qian, C.F., Zhao, M.H., Lee, S.W.R., Tong, P., Zhang, T.Y., 2000. Effects of electric fields on the bending behavior of PZT-5H piezoelectric laminates. *Smart Materials and Structures* 9, 824–831.
- Cheng, J.Q., Wang, B., Du, S.Y., 2000. A statistical model for predicting effective electroelastic properties of polycrystalline ferroelectric ceramics with aligned defects. *International Journal of Solids and Structures* 37 (35), 4763–4781.
- Cheng, J.Q., Wang, B., Du, S.Y., 2002. A statistical model prediction of effective electroelastic properties of polycrystalline ferroelectric ceramics with randomly oriented defects. *Mechanics of Materials* 34 (10), 643–655.
- Cheng, J.Q., Wang, B., Du, S.Y., 2005a. A theoretical analysis of piezoelectric/composite laminate with larger-amplitude deflection effect. Part II: Hermite Differential Quadrature method and application. *International Journal of Solids and Structures* 42 (24–25), 6181–6201.

- Cheng, J.Q., Wang, B., Du, S.Y., 2005b. A theoretical analysis of piezoelectric/composite laminate with larger-amplitude deflection effect. Part I: Fundamental equations. *International Journal of Solids and Structures* 42 (24–25), 6166–6180.
- Cheng, J.Q., Wu, X.X., Li, G.Q., Taheri, F., Pang, S.S., 2006. Development of a smart composite pipe joint integrated with piezoelectric layers under tensile loading. *International Journal of Solids and Structures* 43 (17), 5370–5385.
- Cheng, J.Q., Taheri, F., Han, H.P., 2006. Strength improvement of a smart adhesive bonded joint system by partially integrated piezoelectric patches. *Journal of Adhesive Science and Technology* 20 (6), 503–518.
- Cheng, J.Q., Wu, X.X., Li, G.Q., Pang, S.S., Taheri, F., 2007. Design and analysis of a smart composite pipe joint integrated with piezoelectric layers under bending. *International Journal of Solids and Structures* 44 (1), 298–319.
- Chon, C.T., 1982. Analysis of tubular lap joint in torsion. *Journal of Composite Materials* 16, 268–284.
- Goland, M., Reissner, E., 1944. The stress in cemented joints. *Journal of Applied Mechanics* 11, A17–A27.
- Graves, S.R., Adams, D.F., 1981. Analysis of a bonded joint in a composite tube subjected to torsion. *Journal of Composite Materials* 15, 211–224.
- Harte, A.M., McNamara, U., Roddy, I.D., 2003. Application of optimisation methods to the design of high performance composite pipelines. *Journal of Materials Processing Technology* 142 (1), 58–64.
- Hart-Smith, L.J., 1973. Adhesive-bonded single lap joints. NASA, CR-112236.
- Hart-Smith, L.J., 1983. Designing to minimize peel stresses in adhesive-bonded joints. In: Johnson, W.S. (Ed.), . In: *Delamination and Debonding of Materials*, vol. 876. ASTM STP, pp. 238–266.
- Hashim, S.A., Cowling, M.J., Lafferty, S., 1998. The integrity of bonded joints in large composite pipes. *International Journal of Adhesion and Adhesives* 18 (6), 421–429.
- Hipol, P.J., 1984. Analysis and optimization of a tubular joint subjected to torsion. *Journal of Composite Materials* 18, 298–311.
- Jiang, B., Batra, R.C., 2001. Micromechanical modeling of a composite containing piezoelectric and shape memory alloy inclusions. *Journal of Intelligent Material Systems and Structures* 12 (3), 165–182.
- Kim, J.K., Lee, D.G., 2004. Effects of applied pressure and temperature during curing operation on the strength of tubular single-lap adhesive joints. *Journal of Adhesion Science and Technology* 18 (1), 87–107.
- Lee, C.K., Moon, F.C., 1990. Modal sensors and actuators. *Journal of Applied Mechanics* 57, 434–441.
- Lees, J.M., 2006. Behaviour of GFRP adhesive pipe joints subjected to pressure and axial loadings. *Composites Part A: Applied Science and Manufacturing* 37 (8), 1171–1179.
- Mura, T., 1982. *Micromechanics of Defects in Solids*. Martinus Nijhoff Publishers, The Hague.
- Oh, J.H., 2007. Nonlinear analysis of adhesively bonded tubular single-lap joints for composites in torsion. *Composites Science and Technology* 67, 1320–1329.
- Pugno, N., Carpinteri, A., 2003. Tubular adhesive joints under axial load. *Journal of Applied Mechanics: Transactions of the ASME* 70 (6), 832–839.
- Reddy, J.N., 2004. *Mechanics of Laminated Composite Plate and Shell: Theory and Analysis*, second ed. CRC Press.
- Roberts, T.M., 1989. Shear and normal stresses in adhesive joints. *Journal of Engineering Mechanics* 115 (11), 2460–2479.
- Tan, P., Tong, L.Y., 2001. Micro-electromechanics models for piezoelectric-fiber-reinforced composite materials. *Composites Science and Technology* 61 (5), 759–769.
- Wang, B., 1992. Three-dimensional analysis of an ellipsoidal in a piezoelectric materials. *International Journal of Solids and Structures* 29, 293–308.
- Whitney, J.M., 1987. *Structural Analysis of Laminated Anisotropic Plates*. Technomic Publishing Co. Inc, Lancaster, PA.
- Włodzimierz, K., Przybyłowicz, P.M., 2003. Active stabilisation of a piezoelectric fiber composite shaft subject to follower load. *International Journal of Solids and Structures* 40, 5063–5079.
- Wu, X.X., Cheng, J.Q., Wang, B., 2001. Influence of applied electric field on the energy release rate for cracked PZT/elastic laminates. *Smart Materials and Structures* 10 (5), 970–978.
- Yang, C.D., 2000. Design and analysis of composite pipe joints under tensile loading. *Journal of Composite Materials* 34 (4), 332–349.
- Yang, C.D., Huang, H., Guan, Z.D., 2002. Stress model of composite pipe joints under bending. *Journal of Composite Materials* 36 (11), 1331–1348.
- Zou, G.P., Taheri, F., 2006. Stress analysis of adhesively bonded sandwich pipe joints subjected to torsional loading. *International Journal of Solids and Structures* 43 (20), 5953–5968.